ACS NANO

www.acsnano.org

PERSPECTIVE

Quantum-State Renormalization in Semiconductor Nanoparticles

Jie Chen, Rena C. Kramer, Thomas R. Howell, and Richard A. Loomis*

Cite This: *ACS Nano* 2024, 18, 35104–35118

Read Online

ACCESS | Metrics & More | Article Recommendations

ABSTRACT: **A single photoexcited electron–hole pair within a polar semiconductor nanocrystal (SNC) alters the charge screening and shielding within it. Perturbations of the crystal lattice and of the valence and conduction bands result, and the quantum-confinement states in a SNC shift uniquely with a dependence on the states occupied by the carriers. This shifting is termed quantum-state renormalization (QSR). This Perspective highlights QSR in semiconductor quantum wires and dots identified in time-resolved transient absorption and two-dimensional electronic spectroscopy experiments. Beyond the interest in understanding the principles of QSR and energy-coupling mechanisms, we pose the contributions of QSR in time-resolved spectroscopy data must be accounted for to accurately identify the time scales for intraband relaxation of the carriers within SNCs.**

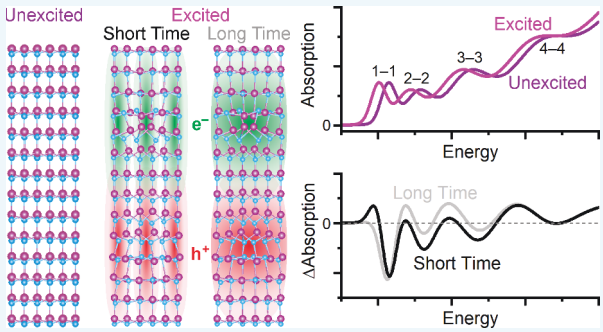

KEYWORDS: *Semiconductor Quantum Nanostructures, Transient Absorption Spectroscopy, Two-Dimensional Electronic Spectroscopy, Quantum-State Renormalization, Band-Gap Renormalization, Fröhlich Interactions, Exciton–Photon Coupling*

OVERVIEW

Semiconductor nanocrystals (SNCs) offer tunability of their optical spectra through control of quantum-confinement effects that depend on their chemical compositions, sizes, and dimensionalities. Significant advances have been made in optimizing synthetic schemes for making high-quality colloidal SNCs with well-defined physical and electronic properties, and SNCs are now being used in impactful applications, including solar cells, lasers, photodetectors, and bioimaging.[1−5] Despite these successes, questions remain concerning the roles that the energies and densities of the quantum-confinement states have on photoluminescence (PL) quantum yields and on the intraband relaxation dynamics of photoexcited carriers. It is common to refer to SNCs as atom-like systems with discrete states and quantized energies. Clearly, the energies of the electron orbitals of a multielectron atom depend on the states occupied since electron screening/shielding and orbital renormalization depend on the electronic configuration of the atom. In this Perspective, we pose that some of the outstanding questions on SNCs are consequences of quantum-state renormalization (QSR), or the energetic shifting of the quantum-confinement states of a SNC induced by photoexcitation, similar to the renormalization that occurs in atoms. We provide an overview of QSR with a focus placed on the contributions of QSR present in data collected in time-resolved optical spectroscopy measurements. We illustrate the need to account for QSR when characterizing the intraband relaxation dynamics of charge carriers within SNCs.

The valence and conduction bands (VB and CB) of a semiconductor are commonly generalized using the effective-mass approximation (EMA),[6,7] where each band is approximated with a parabola scaled inversely with the effective mass of the charge carrier, Figure 1(a)-black. The crystalline properties of and electrostatic interactions within the semiconductor change with photoexcitation, and the effective masses and band structures adjust accordingly. The strong interactions of photoexcited electrons, holes, and excitons with the ions in a polar semiconductor nanocrystal are termed Fröhlich interactions.[8−15] When an electron and hole are bound as an exciton, the equilibrium separation of the electron and hole results in contrasting Coulombic interactions with the lattice ions; the electron(hole) in an exciton attracts(repels) cations(anions). If the exciton radius is notably greater than the lattice constant and if the effective mass of the hole is significantly larger than that of the electron, the interaction can

Received: July 21, 2024
Revised: November 25, 2024
Accepted: December 3, 2024
Published: December 18, 2024

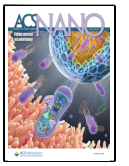

https://doi.org/10.1021/acsnano.4c09833
ACS Nano 2024, 18, 35104–35118

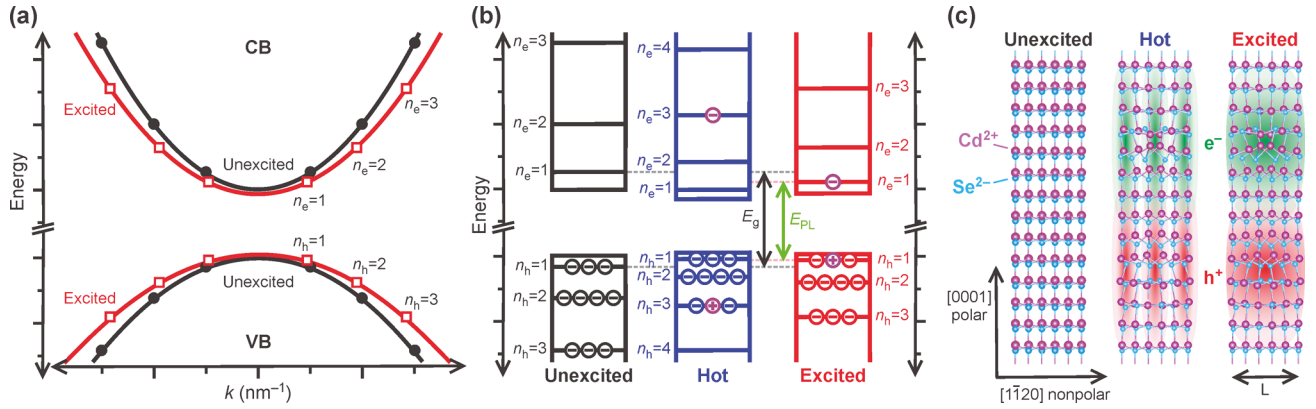

Figure 1. Quantum-state renormalization (QSR). (a) Schematics of the valence and conduction bands, VB and CB, using the effective-mass approximation for an unexcited and excited semiconductor. Only discrete energies and *k* values exist along the bands of semiconductor nanocrystals, symbols. (b) Photoexcitation and QSR results in a shifting of the quantum-confinement states to lower energies in comparison to the unexcited SNC with a dependence on the states occupied by the carriers. The photoluminescence energy, E_{PL}, is Stokes shifted from the band gap energy, E_g, identified in absorption spectra. (c) The crystal structure, shown for a wurtzite CdSe quantum platelet, becomes perturbed with photoexcitation with a dependence on the quantum-confinement states occupied. Note, the number of electrons included in (b) is not suggesting the degeneracy as each of these quantum-confinement states of a SNC with translational degrees of freedom has a continuum of states.

be regarded as the sum of independent interactions of the carriers with optical phonons.[13−19] The effective masses in polar semiconductors usually increase with photoexcitation, causing the bands to broaden and shift energetically closer to each other,[20−22] Figure 1(a)-red. These photoinduced changes termed bandgap renormalization (BGR), were initially associated with a high density or a plasma of electron−hole pairs prepared in the semiconductor,[23−29] but it also occurs with low excitation fluence in the spatial regions near a photoexcited electron/hole pair. The magnitude of BGR depends on the constituents and polarity of the semiconductor, effective masses and Bohr radii of the carriers, exciton binding energy, and dimensionality and size of the semiconductor.[26]

As the size of a SNC is reduced to nanometers in at least one dimension, quantum confinement results in discrete states at equal intervals of *k* along each parabolic band, symbols in Figure 1(a).[6,7] These quantized levels can also be depicted using one-dimensional particle-in-a-box (1DPIB) diagrams, Figure 1(b)-black for the unexcited SNC. It is the transitions between these states that contribute to the steady-state absorption, $Abs_{SS}(E)$, spectrum. The states of an unexcited SNC are ultimately dictated by the constituents and properties of the semiconductor crystal lattice, as depicted in Figure 1(c)-left for a wurtzite CdSe 1D quantum platelet (QP).

The photoexcitation of the SNC shifts each quantum-confinement state by a unique energy, ΔE_{QSR}, Figure 1(b)-middle and right, that depends on the states occupied by the carriers due to their dissimilar wave functions. Consequently, the EMA breaks down for an excited SNC as the energies of the states do not fall along a single parabolic band. Photoexcitation of the $n_e = 3 - n_h = 3$ transition of a QP prepares an electron and hole in states with two nodes in the wave functions along the confinement direction, Figure 1(c)-middle panel. Once the carriers relax to the band-edge states, Figure 1(c)-right, the interactions of the carriers with the crystal lattice change due to the contrasting spatial distributions of the wave functions. Ultimately, the lowest-energy states from which the carriers may undergo radiative recombination, $n_e = 1$ and $n_h = 1$ for 1DPIB systems, are each perturbed by ΔE_{QSR}, and the PL occurs at lower energies than those of the band gap absorption feature, i.e., there is a Stokes shift associated with QSR. The unique shifting of the quantum-confinement states is QSR, and it can be likened to state-specific BGR.

TIME-RESOLVED OPTICAL SPECTROSCOPY OF SEMICONCUDTOR NANOCRYSTALS

Time-resolved, transient absorption (TA) spectroscopy is often implemented to characterize the intraband relaxation of carriers in SNCs.[30−50] TA experiments collect the differential absorption spectra between the photoexcited and unexcited sample across a wide energy region as a function of time. Contributions from QSR are present in the TA data, but they are typically not considered or characterized. The types of optical transitions that contribute to TA data of a sample of SNCs, $\Delta Abs_{TA}(E, t)$, are illustrated in Figure 2(a). Transitions between the quantum-confinement states of an unexcited SNC dominate the profile of an $Abs_{SS}(E)$ spectrum, Figure 2(b)-top. The states energetically shift with photoexcitation due to QSR, and the transitions in the $Abs_{SS}(E)$ spectrum become bleach transitions, BL_{QSR}, Figure 2(a)-dashed arrows, that do not shift with time. The sum of the BL_{QSR} features results in $BL_{QSR}(E, t)$ spectra that remain as long as there is an excited electron or a hole remaining in the SNC. Transitions between the shifted states are induced-absorption, IA, transitions that make up $IA_{QSR}(E, t)$ spectra with properties that depend on the states occupied by the carriers, Figure 2(b)-middle. At long times, the carriers in an excited SNC populate the shifted band-edge states, and the lowest-energy feature in the $IA_{QSR}(E, t)$ spectra is at the same energy as the peak of the $PL(E)$ spectrum. The contributions of the $IA_{QSR}(E, t)$ remain in the $\Delta Abs_{TA}(E, t)$ data as long as there are excited carries in the SNC, but the transition energies shift independently with time as the carriers undergo intraband relaxation. The contributions from QSR in a TA measurement, $\Delta Abs_{QSR}(E, t)$, are a sum of the positive $IA_{QSR}(E, t)$ and negative $BL_{QSR}(E, t)$ signals, and derivative-like spectra result.

Absorptive interband transitions between shifted states occupied by either an electron or hole become less likely for an excited SNC, especially for quantum dots (QDs) due to

https://doi.org/10.1021/acsnano.4c09833
ACS Nano 2024, 18, 35104−35118

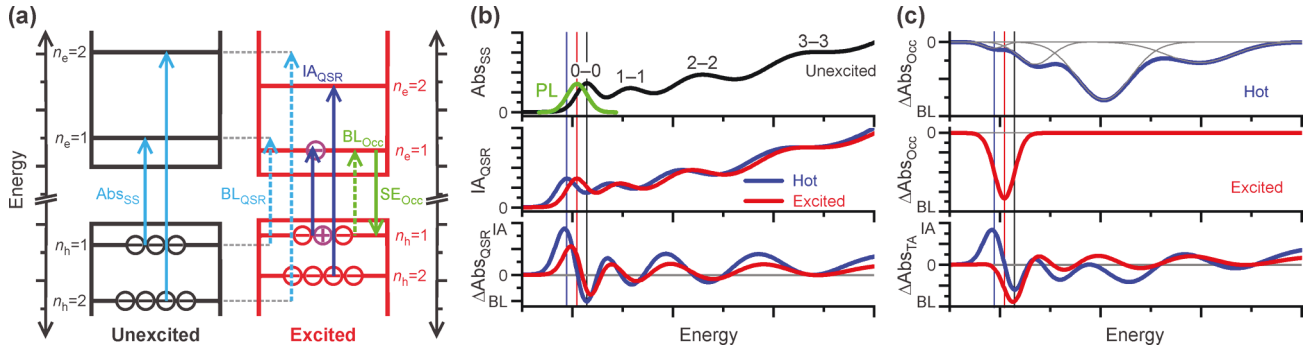

Figure 2. Spectroscopy of SNCs. (a) The transitions that contribute to $Abs_{SS}(E)$ and $\Delta Abs_{TA}(E, t)$ spectra of SNCs are illustrated in the 1DPIB diagrams for the unexcited and excited SNCs. (b) The $Abs_{SS}(E)$, black, is dominated by excitonic transitions between quantum-confinement states. Electron−hole radiative recombination occurs from the shifted lowest-energy states, and the photoluminescence spectrum, PL(E)-green, is Stokes shifted below the band gap feature in the $Abs_{SS}(E)$ spectrum. The quantum-confinement states in excited and highly excited SNCs shift due to QSR, and $IA_{QSR}(E, t)$ spectra, middle, that depend on the states occupied result. The contributions from QSR in $\Delta Abs_{TA}(E, t)$ spectra are $\Delta Abs_{QSR}(E, t) = IA_{QSR}(E, t) - Abs_{SS}(E)$, plotted in bottom panel. (c) Carriers occupying the shifted states give rise to BL signals, ΔAbs_{Occ}. For photoexcitation above the band-edge states, the carriers occupy energetically excited states at short times, top. The carriers relax to the band-edge states with time, middle. The data collected in a TA experiment are $\Delta Abs_{TA}(E, t) = \Delta Abs_{QSR}(E, t) + \Delta Abs_{Occ}(E, t)$, bottom.

Pauli blocking. These transitions become bleach signals, $BL_{Occ}(E, t)$, that make up the occupancy spectra, $\Delta Abs_{Occ}(E, t)$, that contribute to the $\Delta Abs_{TA}(E, t)$ data. It is possible for stimulated emission, $SE_{Occ}(E, t)$, to occur, but these signals only become measurable with high excitation fluences[51] and are indistinguishable from the $BL_{Occ}(E, t)$ signals. The relative intensities of the features in the $\Delta Abs_{Occ}(E, t)$ spectra track the populations of the carriers in the different states as they relax with time from the prepared highly excited states within the SNC to the lowest-energy, excited states, as depicted in Figure 2(c)-top and middle, respectively.

The $\Delta Abs_{TA}(E, t)$ data for SNCs contain the sum of the $\Delta Abs_{QSR}(E, t)$ and $\Delta Abs_{Occ}(E, t)$ signals, Figure 2(c)-bottom. The short-time $\Delta Abs_{TA}(E, t)$ data obtained for highly excited SNCs, photoexcitation of a single electron−hole pair well above the band gap states, contain contributions from $\Delta Abs_{QSR}(E, t)$ throughout the spectral region and $\Delta Abs_{Occ}(E, t)$ signals associated with the higher-energy transitions, blue spectrum. The positive $\Delta Abs_{TA}(E, t)$ signals present below the steady-state band gap feature observed at short times are associated with the $IA_{QSR}(E, t)$ signals of the shifted band-edge states and not with biexcitons.[35,49,50,52−65] This discrepancy will be discussed in more detail below. At longer times, the electron and hole each relax into the shifted band-edge states, and the $BL_{Occ}(E, t)$ signals of these carriers negate the low-energy $IA_{QSR}(E, t)$ signals, red in Figure 2(c)-bottom. These low-energy $IA_{QSR}(E, t)$ signals would not be observed if exciting directly into the band-edge states as the $BL_{Occ}(E, t)$ signals would promptly cancel them. Ultimately, the strong BL signals in the $\Delta Abs_{TA}(E, t)$ data observed near the steady-state band-edge energy at longer times are dominated by the $BL_{QSR}(E, t)$ signals of the band-edge states. The undulations in the $\Delta Abs_{TA}(E, t)$ data at higher energies and longer times are due to $\Delta Abs_{QSR}(E, t)$. Once the carriers are in the lowest-energy states, all of the signals in the $\Delta Abs_{TA}(E, t)$ data decay with the population of the carriers within the SNC.

BANDGAP RENORMALIZATION IN SEMICONDUCTOR NANOMATERIALS

Transition Metal Dichalcogenides. Recent investigations have probed the BGR in transition metal dichalcogenides (TMDs).[66−69] Pogna, et. al[66] probed BGR in single-monolayer (1 ML) MoS_2 using steady-state absorption and TA measurements. The $Abs_{SS}(E)$ spectrum of a 1 ML MoS_2 crystal, Figure 3(a),[66] contains three peaks associated with the A, B, and C excitonic transitions with the band gap feature centered at 1.90 eV. There are no detectable transitions between other, higher-energy quantum-confinement states within these bands. The $\Delta Abs_{TA}(E, t)$ spectra at short time, t = 300 fs, acquired with photoexcitation at excitation energies of E_{exc} = 3.10, 2.06, and 1.88 eV contain differential absorption signals that simultaneously appeared throughout the spectral window, regardless of the excitation energy, Figure 3(b).[66] The $\Delta Abs_{TA}(E, t)$ spectra contain BL signals at the energies of the steady-state excitonic features, and significant IA signals below the band gap energy, much like the model $\Delta Abs_{TA}(E, t)$ spectrum, blue in Figure 2(c)-bottom. These $IA(E, t)$ features are associated with the A excitonic feature, which is shifted by BGR, prior to carriers relaxing into these states. The authors concluded there is a dynamic BGR in the 1 ML MoS_2 crystals caused by the presence of photoexcited carriers.[66]

These conclusions are in agreement with the results of Lin et al.,[67,68] who probed the ultrafast excitation-induced BGR in 1 ML MoS_2 on a conducting substrate using extreme-ultraviolet time-resolved angle-resolved photoemission spectroscopy. In those experiments,[67,68] the MoS_2 was photoexcited with 2.2 eV photons and the momentum-dependent changes in the CB and VB energies and effective masses, i.e., the BGR of the bands, were quantitatively characterized as a function of time after photoexcitation and the density of photoexcited carriers. They were able to identify an increase of 40 meV in the band gap energy at the K point that recovered with a decay time constant of ~5 ps. In contrast, the energy separation of the CB and VB at the edge of the discernible valley ($k = k_{valley\ edge}$) decreased by ~100 meV with a slower recovery time. The experiments were supported by high-level theory, and they identified the contributions to the BGR from excitons versus separate electrons and holes. Ultimately, this research[67,68] provided convincing evidence for BGR in 1 ML MoS_2.

Perovskites. Due to noteworthy advances in terms of making colloidal halide perovskites with excellent optical properties, including large absorption coefficients, tunable

https://doi.org/10.1021/acsnano.4c09833
ACS Nano 2024, 18, 35104−35118

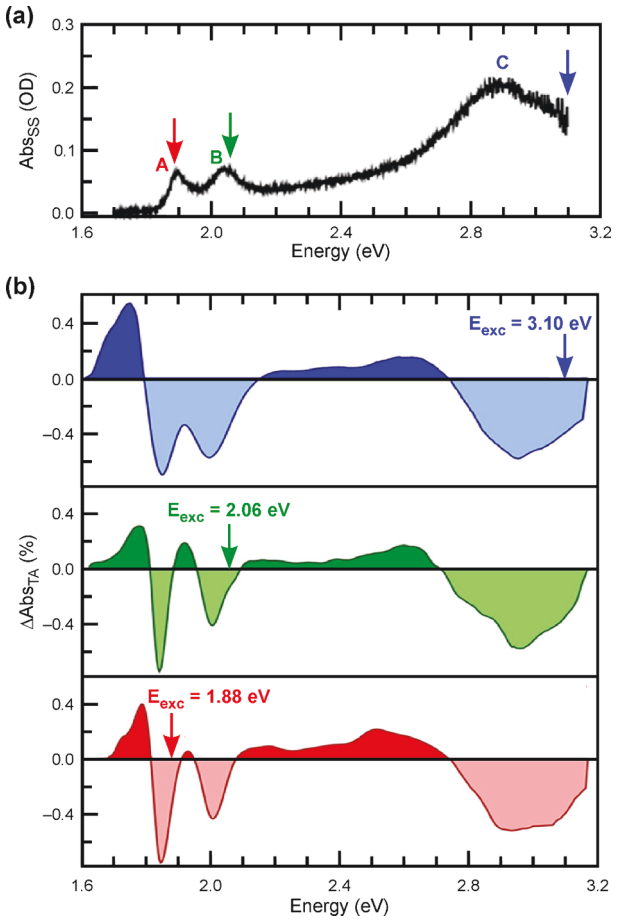

Figure 3. QSR in monolayer MoS_2. (a) The $Abs_{SS}(E)$ spectrum of a 1 ML MoS_2 single crystal is plotted with three excitonic features labeled. (b) TA spectra of the 1 ML MoS_2 were acquired at a delay of 300 fs using the indicated excitation energies, E_{exc}. This figure was adapted with permission from ref 66. Copyright 2016 American Chemical Society.

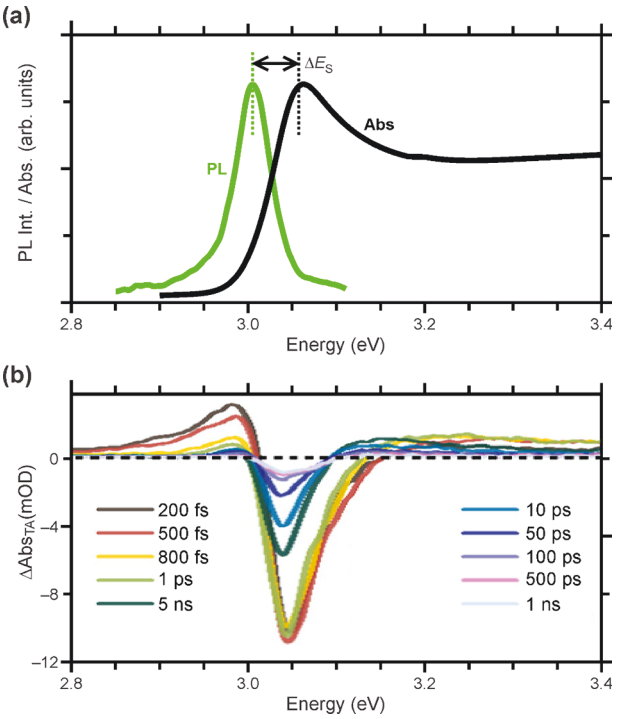

Figure 4. Spectroscopic data measured on ~10 nm cubic $CsPbCl_3$ NCs at room temperature. (a) There is a Stokes shift of ~50 meV between the $Abs_{SS}(E)$ (black) and $PL(E)$ spectra. These spectra were digitized from Figures 1(a) and Supplementary Information Figure S3(a), respectively.[87] (b) The TA data were collected with excitation at 4.42 eV with low fluences; the average number of electron−hole pairs excited per pulse was ~0.05. These TA data were scanned from Figure 2(a).[87] These figures were adapted with permission from ref 87. Copyright 2023 American Chemical Society.

absorption and emission energies, high PL quantum yields, and long carrier diffusion lengths,[70] these semiconductor nanomaterials have already been incorporated in high-performance photovoltaics.[71,72] Despite these developments in halide perovskite materials, numerous questions related to carrier relaxation and trapping dynamics, their structural and chemical stabilities, and the roles of carrier-phonon coupling remain. A growing body of work has provided strong evidence for excitation-induced BGR in perovskite materials with varying molecular and ionic compositions.[70,73−89]

Shukla et al.[87] investigated the temperature and excitation-energy dependence of BGR in $CsPbCl_3$ nanocrystals (NCs). Their spectroscopic data highlighting the BGR of room-temperature $CsPbCl_3$ cubic NCs with sizes of ~10 nm are included in Figure 4.[87] The room-temperature $Abs_{SS}(E)$ spectrum of a film of the NCs has a prominent exciton peak just above 3.05 eV, black, and the $PL(E)$, green, is Stokes shifted by ~50 meV, as shown in Figure 4(a). The authors carefully analyzed the room-temperature $PL(E)$ and identified five contributing features with intensities, energies, and number of features being dependent on temperature.[87] These features are associated with bound excitons, free excitons, and biexcitons.

Room-temperature TA data collected for the $CsPbCl_3$ NCs with excitation at 4.42 eV and low fluences are plotted in Figure 4(b),[87] and these are typical of the type and quality of the data reported for perovskite NCs.[70,73−89] The prominent features present in these TA data are similar to those presented in Figure 3(b) for 1 ML MoS_2.[66] There is a prominent $BL(E, t)$ feature near 3.05 eV associated with band gap exciton transitions that remains as long as there are carriers present within the NCs, > 1 ns. There is an $IA(E, t)$ feature to lower energies that decays on shorter time scales, within ~1 ps. The authors attribute this feature to probe laser-induced biexciton transitions,[87] but we and others[73−83] associate these signals with BGR caused by the excitation pulse. There are also broad $IA(E, t)$ signals to higher energies that remain for longer times, >1 ns. These signals are similar to those in the central energy region of the MoS_2 data.[66] The $Abs_{SS}(E)$ data for the MoS_2 and $CsPbCl_3$ NCs contain no excitonic or quantum-confinement features in these regions.

The photoexcitation of the $CsPbCl_3$ NCs with highly energetic photons creates hot carriers at energies well above the band gap states. The photoinduced changes within the VB and CB give rise to BGR and a shifting of the band-edge exciton states to lower energies.[75] This band shifting results in the generation of $IA(E, t)$ features at energies below the band gap and $BL(E, t)$ features associated with the unperturbed band-edge states. A derivative profile near the band gap is consequently observed in time-resolved TA measurements at short times. The $IA(E, t)$ feature becomes negated with time as

https://doi.org/10.1021/acsnano.4c09833
ACS Nano 2024, 18, 35104−35118

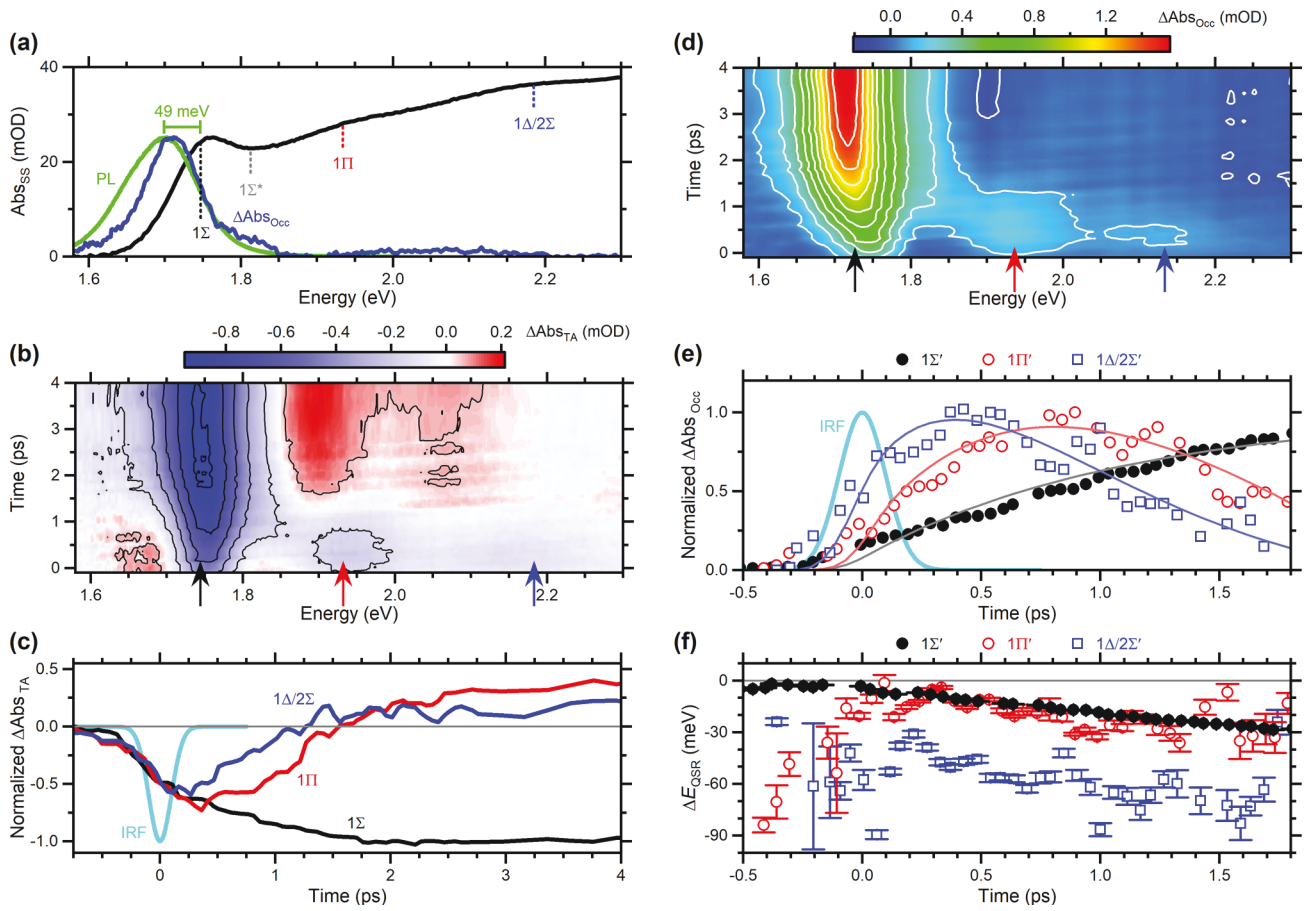

Figure 5. TA and occupancy data collected on wurtzite CdTe QWs. (a) The $Abs_{SS}(E)$ spectrum of the CdTe QWs contains numerous exciton features, which are labeled using the electron quantum-confinement states accessed in the CB. The PL(E) spectrum, recorded with excitation at 2.76 eV, has a maximum that is 49 meV below the centroid of the lowest-energy 1Σ absorption feature. The long-time, t = 7 ns, $\Delta Abs_{OCC}(E, t)$ spectrum is nearly identical to the PL(E) spectrum, indicating the carriers are predominantly in the shifted band-edge states. (b) The $\Delta Abs_{TA}(E, t)$ data collected with excitation at 2.76 eV contain overlapping BL(E, t) (blue) and IA(E, t) (red) signals. (c) The temporal profiles of the $\Delta Abs_{TA}(E, t)$ data at the energies of the 1Σ, 1Π, and 1Δ/2Σ absorption features, indicated by arrows in b, appear as BL signals on the same time scales because of contributions from QSR. The instrument response function is also plotted. (d) $\Delta Abs_{Occ}(E, t)$ data, obtained as described in refs 30, 31, and 47, indicate the presence of carriers in the different shifted states. (e) The temporal profiles of the shifted 1Σ′, 1Π′, and 1Δ/2Σ′ occupancy features reveal the time scales for intraband relaxation. (f) The energies of the occupancy features shift independently with time after photoexcitation. These results were reported in ref 31.

the photoexcited carriers relax into these shifted states, and only the BL(E, t) feature associated with the unperturbed band-edge states remains. The decay of the amplitude of the below-gap IA(E, t) feature indicates the intraband relaxation of the carriers to the shifted band-edge states of the $CsPbCl_3$ NCs occurs within ∼1 ps, Figure 4(b). We propose the broad continuum IA signals observed at higher energies have contributions from BGR of the higher-energy continuum states accessed in the $Abs_{SS}(E)$ spectra throughout this energy region. There may also be contributions in these IA signals from photoinduced changes in the refractive index of the $CsPbCl_3$ NCs.[73,75,77]

There are also several reports on BGR in perovskite materials with varying chemical compositions and morphologies. Soetan et al.[83] determined the BGR decreased, from 180 to 110 meV, with increasing Cl content in $CsPb(Br_xCl_{1-x})_3$ mixed-halide perovskite NCs. Telfah et al.[76] measured similar BGR for methylammonium lead bromide perovskite nanostructures with (0D) nanocrystal, (1D) nanowire, and (2D) nanoplatelet morphologies. In contrast, Yan et al.[80] measured giant and contrasting BGR energies of 480 and 336 meV for $CsPbBr_3$ microrods and microplates, respectively. These reports indicate there are many factors that contribute to the BGR of perovskites and continued investigations are needed to create a better understanding of the photoinduced changes.

QUANTUM-STATE RENORMALIZATION IN CdTe QUANTUM WIRES

The $Abs_{SS}(E)$ spectra of II−VI and III−V SNCs typically contain numerous excitonic features associated with transitions between the quantum-confinement states within the VB and CB. The electron−hole interactions are strong in semiconductor quantum wires (QWs) due to confinement in two dimensions, and photoexcited electron−hole pairs can remain bound as 1D excitons in high-quality QWs.[31,90,91] Fröhlich interactions and exciton−phonon interactions can be large enough to form exciton polarons that are spatially larger than the lattice constant of the semiconductor.[92−94] In addition, the lowest-energy fine-structure states in QWs are optically bright,[95,96] and the energies of the $SE_{Occ}(E, t)$ signals would be the same as of the $BL_{Occ}(E, t)$ signals. The intensities of both of these negative signals in the $\Delta Abs_{TA}(E, t)$ data would

https://doi.org/10.1021/acsnano.4c09833
ACS Nano 2024, 18, 35104−35118

be proportional to the number of carriers in the states. For these reasons, semiconductor QWs are well-suited systems for investigating QSR.

The results obtained for colloidal wurtzite CdTe QWs with a PL quantum yield of 8.8% and reported in ref 31 are summarized in Figure 5. The $Abs_{ss}(E)$ spectrum of these QWs, Figure 5(a), contains inhomogeneously broadened excitonic features with each comprised of numerous transitions that tend to access the same electron quantum-confinement states, which are labeled. The ensemble $PL(E)$ spectrum is Stokes shifted by ΔE_S = 49 meV from the lowest-energy 1Σ feature. The $\Delta Abs_{TA}(E, t)$ data for these CdTe QWs, which were collected using photoexcitation at E_{exc} = 2.7 eV and low excitation fluences, are plotted in Figure 5(b). These $\Delta Abs_{TA}(E, t)$ data are typical for most SNCs with a strong $BL(E, t)$ feature, blue, near the energy of the band-edge energy, an $IA(E, t)$ feature, red, to lower energies that lasts for <1 ps, and additional $BL(E, t)$ and $IA(E, t)$ features to higher energies that remain as long as there are carriers in the SNC. The temporal profiles of the $\Delta Abs_{TA}(E, t)$ data at the energies of the three prominent features within the $Abs_{SS}(E)$ spectrum, indicated by arrows below Figure 5(b), are plotted in Figure 5(c). All three profiles begin as negative BL signals that appear on the same time scale; the appearance of the 1Σ $BL(E, t)$ feature fits to a single-exponential function with a time constant of 0.98(2) ps.[31] The signals near the 1Π and 1Δ/2Σ energies, however, become positive IA signals within 2 ps. The short-time BL near the 1Π feature is centered at the same energy as observed in the $Abs_{SS}(E)$ spectrum, but it shifts to lower energies once it becomes an IA signal. The complicated nature of the $\Delta Abs_{TA}(E, t)$ data is associated with the overlapping contributions from the $\Delta Abs_{QSR}(E, t)$ and $\Delta Abs_{Occ}(E, t)$ signals.

A simple model[30,31,47] that utilizes the $Abs_{SS}(E)$ of a SNC sample and assumes all of the quantum confinement states shift by the same energy was implemented to approximate the $\Delta Abs_{QSR}(E, t)$ contributions within the $\Delta Abs_{TA}(E, t)$ data and to extract the $\Delta Abs_{Occ}(E, t)$ data, Figure 5(d). The assumption the states experience the same QSR is not valid, but it does enable much of the contributions from the $BL_{QSR}(E, t)$ and $IA_{QSR}(E, t)$ to be approximated. At long times, >4 ps, after the photoexcited carriers relaxed to the 1Σ′ shifted band-edge states, the shapes of the $\Delta Abs_{Occ}(E, t)$ spectra remain the same, Figure 5(a)-blue. The prime indicates that state has shifted with photoexcitation. The peak energy of the 1Σ′ $\Delta Abs_{Occ}(E, t)$ spectra at long times is the same as the maximum of the $PL(E)$ spectrum. This is direct evidence that the Stokes shift of the $PL(E)$ spectrum has a significant component from QSR of the band-edge states. Second, the agreement indicates the energetic shift is not associated with biexcitons, which would not be present at long times after photoexcitation.

The $\Delta Abs_{Occ}(E, t)$ spectrum at each time was fit to a sum of Gaussians,[30,31,47] one for each shifted excitonic feature, and the integrated area of each Gaussian is proportional to the population of carriers in those states. The time-dependences of the populations in the different states, Figure 5(e), track the intraband relaxation of the carriers. Once QSR is approximately accounted for, the time scales for carriers populating the different features are significantly longer than the appearance times of the $\Delta Abs_{TA}(E, t)$ features; the appearance time of the 1Σ feature in the $\Delta Abs_{TA}(E, t)$ data is 0.98(2) ps while that of the shifted 1Σ′ occupancy feature is nearly twice as long, 1.90(4) ps.[31] The centroid energies of the occupancy features are observed to shift independently with time, Figure 5(f). The energy of the 1Σ′ feature begins just below the energy of the steady-state 1Σ absorption feature, and it continues to shift to >30 meV as the carriers relax into the band-edge states. In contrast, the energy of the 1Π′ feature is ∼85 meV below the energy of the steady-state 1Π absorption feature during the excitation pulse, then quickly shifts to only ∼10 meV, and ultimately increases to a shift of 32 meV by 1.8 ps. This dynamic behavior of the quantum-confinement states indicates: (i) all of the states do not shift by the same energy with time, as assumed in the simple model[47] used to analyze the data; (ii) QSR is more than just BGR since the energies of the states shift independently with time; and (iii) the amount of QSR depends on the states occupied by carriers within the SNC.

QUANTUM-STATE RENORMALIZAITON IN QUANTUM DOTS

Colloidal semiconductor QDs, with three-dimensional quantum confinement and no translational degrees of freedom for the carriers, offer contrasting carrier relaxation dynamics, energetics, densities of states, and carrier−carrier interactions in comparison with those of QWs. Experiments probing QSR and carrier dynamics in colloidal CdSe/ZnS core/shell QDs were recently undertaken in our laboratory.[97] The $Abs_{SS}(E)$ spectrum of these QDs, Figure 6(a), contains the well-characterized features associated with transitions between electron and hole confinement states and indicates a band gap energy of ∼2.004 eV. The $PL(E)$ spectrum is Stokes shifted by ΔE_S = 38 meV, and a PL quantum yield of 37% was measured with excitation at 2.48 eV. $\Delta Abs_{TA}(E, t)$ data were collected using E_{exc} = 2.60 and 2.00 eV and low excitation pulse fluences, <20 μJ cm^{-2}, to limit contributions from multiple carriers within each QD.

The $\Delta Abs_{TA}(E, t)$ data collected for the CdSe/ZnS QDs with E_{exc} = 2.60 eV, Figure 6(b),[97] are typical to those for the CdTe QWs and other SNCs reported in the literature. The properties of the transient signals are emphasized in the $\Delta Abs_{TA}(E, t)$ spectra measured at short and midtimes, t = 0.20 and 2.00 ps, Figure 6(c)-top, and the temporal profiles of the $\Delta Abs_{TA}(E, t)$ data at the three probe energies indicated with arrows, Figure 6(d)-top. There is a prominent BL_{QSR} feature near the energy of the steady-state $1S_{3/2}-1S_e$ band-edge peak, a short-lived IA_{QSR} feature at lower energies, ∼1.93 eV, and long-lived IA_{QSR}, BL_{QSR}, and BL_{Occ} signals features to higher energies. The differences in the amplitudes and energies of the features within the time-dependent spectra, Figure 6(c)-top, are associated with both carrier occupancy and dynamic QSR of the states as the carriers relax through different quantum-confinement states to the band-edge states. The prompt rise of the positive IA_{QSR} signal at 1.93 eV, black in Figure 6(d)-top, is associated with QSR of the band-edge states. The carriers relax into these states within 2 ps, after which the BL_{Occ} signals cancel the IA_{QSR} signals. The properties of the $\Delta Abs_{TA}(E, t)$ spectra remain the same at long times with an overall decay that tracks with the population of carriers remaining in the QDs.

The $\Delta Abs_{TA}(E, t)$ spectra recorded with excitation at the band gap, E_{exc} = 2.00 eV,[97] exhibit very little changes in the relative intensities of the features with time, Figure 6(c)-bottom and 6(d)-bottom. There are no IA_{QSR} signals observed below the band-edge energy since the electrons and holes are

https://doi.org/10.1021/acsnano.4c09833
ACS Nano 2024, 18, 35104−35118

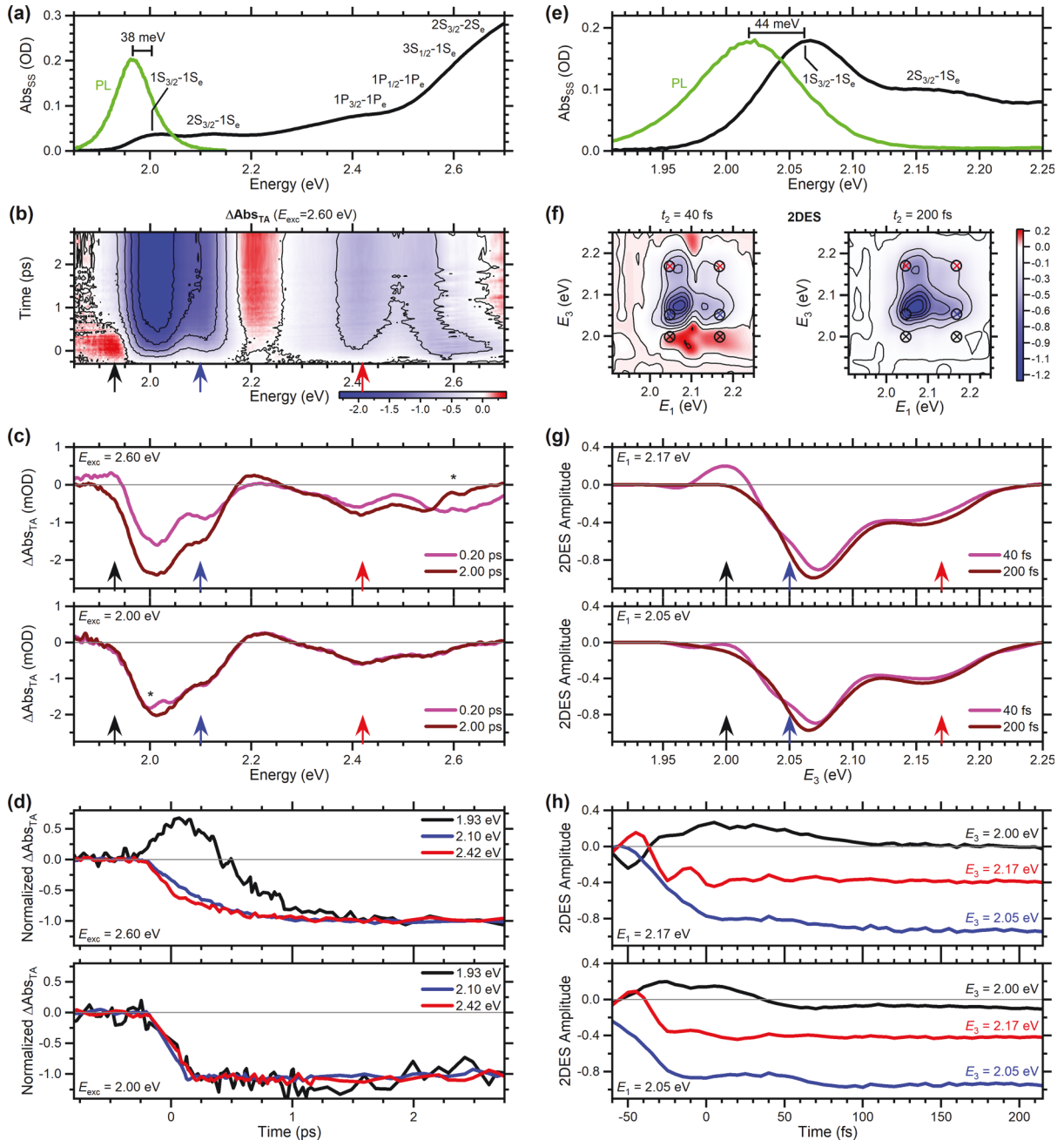

Figure 6. Time-resolved data collected on CdSe/ZnS and CdSe QDs. (a) $Abs_{SS}(E)$ and $PL(E)$ spectra of CdSe/ZnS QDs. (b) TA data of the CdSe/ZnS QDs recorded with E_{exc} = 2.60 eV. (c) TA spectra recorded at the indicated delay times with E_{exc} = 2.60 and 2.00 eV. An * indicates excitation scattering. (d) The temporal profiles at three different probe energies indicated by the arrows in (c), 1.93 eV (black), 2.10 eV (blue) and 2.42 eV (red), are shown for E_{exc} = 2.60 and 2.00 eV. (e) $Abs_{SS}(E)$ and $PL(E)$ spectra of CdSe QDs. (f) 2DES data of CdSe QDs at t_2 = 40 and 200 fs. E_1 is the 2DES excitation energy, E_3 is the emission energy, and t_2 is the time between the excitation and probe pulses. Six peaks within the 2DES spectra are marked with ×. (g) 2DES amplitude spectra for E_1 = 2.17 and 2.05 eV plotted versus E_3 for t_2 = 40 and 200 fs. (h) The temporal profiles of the 2DES amplitudes of the identified peaks. Data for (e)−(h) were published in a different form in ref 106 and obtained from the authors, Brosseau et al.

directly excited into these band-edge states, and the corresponding BL_{Occ} signals promptly cancel the IA_{QSR} signals. These IA signals would still be present if they were a result of biexciton transitions. The shapes of the $\Delta Abs_{TA}(E, t)$ spectra at higher energies are associated with only IA_{QSR} and BL_{QSR}, and all of the TA signals decay with the carrier population in the QDs.

Extensive attempts were made to separate the contributions from QSR and carrier occupancy within the $\Delta Abs_{TA}(E, t)$ collected on these QDs using the simple QSR model[47] as well as more advanced models, but the results were not satisfactory. The primary issues were the energies of most of the IA_{QSR} and BL_{Occ} features do not shift together, and the amount of QSR for each feature seems to separately depend on the states occupied by the electrons and holes. For instance, the two lowest-energy features, associated with the $1S_{3/2}-1S_e$ and $2S_{3/2}-1S_e$ transitions, are observed to shift by dissimilar energies. Since these transitions share a common electron state

https://doi.org/10.1021/acsnano.4c09833
ACS Nano 2024, 18, 35104−35118

and different hole states, the energetic shifts of the hole states are dissimilar. These results emphasize the state shifting cannot be solely associated with BGR, but are better characterized as QSR where the state shifting depends on the probability densities of the states and what states are occupied by carriers.

QUANTUM-STATE RENORMALIZATION IN TWO-DIMENSIONAL ELECTRONIC SPECTROSCOPY

Four-wave mixing techniques, such as time-resolved two-dimensional electronic spectroscopy (2DES), are well suited for exploring the energetics and dynamics of charge carriers in SNCs.[61,62,98−105] Typical 2DES data contain on-diagonal BL(E, t) features associated with transitions to excitonic states of the unexcited SNCs at short times, and these may shift below the diagonal with time.[61,62,98−102] Off-diagonal BL(E, t) features or cross-peaks lying above and below the diagonal are also present in the data, and these are typically associated with interactions or couplings between states.[61,62,98−102] Cross peaks below the diagonal can also be associated with relaxation of carriers from higher-energy states to lower-energy states.

We propose the accounting for QSR in the 2DES data collected on SNCs would likely change some of the conclusions drawn. The high-quality 2DES results obtained by Brosseau et al.[106] on colloidal CdSe QDs are highlighted here. The low-energy region of the $Abs_{SS}(E)$ spectrum of the CdSe QDs contains two features associated with the $1S_{3/2}-1S_e$ and $2S_{3/2}-1S_e$ transitions, and the peak of the PL(E) spectrum is Stokes shifted by ΔE_S = 44 meV,[106] Figure 6(e). The 2DES experiments were performed using 17 fs pulses and a spectral bandwidth of ∼250 meV, spanning the $1S_{3/2}-1S_e$ and $2S_{3/2}-1S_e$ features. The 2DES spectra for pump−probe delay times of t_2 = 40 and 200 fs are plotted in Figure 6(f), and slices of the 2DES spectra along the emission energy, E_3, are plotted for excitation energies of E_1 = 2.17 and 2.05 eV in Figure 6(g). The temporal profiles of the peaks identified in Figure 6(f) are plotted in Figure 6(h).

Similar to the TA results just described for CdSe/ZnS QDs, the 2DES spectra of the CdSe QDs for excitation at the $2S_{3/2}-1S_e$ energy, E_1 = 2.17 eV, at short t_2 contain IA signals at E_3 values below the band gap, ∼2.00 eV,[106] magenta spectrum in Figure 6(g)-top. We propose this IA feature is associated with $1S_{3/2}-1S_e$ transitions that have shifted because of QSR. This E_1 excitation energy results in some BL_{Occ} signal associated with electrons in the shifted $1S_e$ state that partially cancels the IA_{QSR} signal of the shifted $1S_{3/2}-1S_e$ transition. As holes quickly relax from the $2S_{3/2}$ state to the $1S_{3/2}$ state, within ∼100 fs, the contribution from the BL_{Occ} of the shifted $1S_{3/2}-1S_e$ transition increases, canceling this IA_{QSR} signal, burgundy spectrum in Figure 6(g)-top. There is a very weak, extremely short-lived IA signal near E_3 = 2.00 eV for excitation of the band-edge states, E_1 = 2.05 eV, as shown in Figure 6(g)-bottom and 6(h)-bottom. Since this excitation is on the $1S_{3/2}-1S_e$ transition, a prompt canceling of the IA_{QSR} signal by the BL_{Occ} signal of the carriers. The short lifetime, <40 fs, of this signal may be representative of the time scale for the QSR and coupling of the carriers with the crystal lattice.

The 2DES amplitudes for the CdSe QDs with E_1 = 2.05 and 2.17 eV remain beyond 200 fs as BL_{QSR} signals at E_3 = 2.05 and 2.17 eV.[106] Since all quantum-confinement states experience QSR when there are excited carriers within a SNC, there should be cross peaks associated with the shifted states that are not directly occupied by the E_1 excitation. The cross peaks above and below the diagonal will have different temporal dependences since those below the diagonal can have contributions from carrier relaxation and BL_{Occ}. We hypothesize that it may be possible to separate the contributions from QSR and carrier occupancies in the different states through detailed comparisons of the amplitudes and temporal profiles of the cross peaks. The 2DES data collected on the CdSe QDs illustrates the differences in the profiles of the cross peaks. The upper cross peak, E_1 = 2.05 eV, E_3 = 2.17 eV, red in Figure 6(h)-bottom, should have contributions from QSR, with $BL_{QSR}(E, t)$ dominating. Thus, the rise time of this peak can be associated with QSR. In contrast, the lower cross peak, E_1 = 2.17 eV, E_3 = 2.06 eV, blue in Figure 6(h)-top, should also have contributions from $BL_{Occ}(E, t)$. Thus, the difference between the temporal profiles of these peaks should more accurately reveal the time scale for relaxation of holes from the $2S_{3/2}$ to $1S_{3/2}$ state.

HISTORIC INTEPRETATIONS

Biexcitons. The short-lived IA(E, t) signals at just lower energies than the band gap energy are often referred to as excited-state absorption (ESA) features associated with biexciton transitions.[35,53−65] In reviewing the literature, we find the meaning of the term biexciton to be particularly unclear or inconsistent. Historically, a biexciton in a semiconductor referred to two excitons, thus two electrons and two holes, bound to each other through Coulombic interactions.[59,107−112] This scenario is particularly relevant when performing experiments with high excitation fluences, so that multiple electron−hole pairs can be prepared and interact within a single SNC. This low-energy IA(E, t), or ESA, feature present at short times in TA or 2DES spectra can even be observed with low excitation fluences, thereby minimizing contributions from bound biexcitons or multiexcitons, but it is still typically referred to as a biexciton feature.[35,53−64] These biexciton features are associated with the transition energies of an electron−hole pair in those SNCs that are already excited. As such, these spectral features would be present in nonlinear spectroscopy measurements incorporating multiple laser pulses to excite and probe the dynamics of the carriers. Furthermore, the biexcitons are short-lived due to Auger relaxation, and radiative recombination is assumed to occur from the lowest-energy exciton states thermally occupied by the carriers. This interpretation of biexcitons has been broadly adopted in the literature and was thoroughly reviewed by Klimov.[54]

The QSR model, on the other hand, assumes the quantum-confinement states shift uniquely after photoexcitation with dependences on the states occupied by the electron and hole as they relax to the band-edge states. This dynamic state shifting is probed by the second laser in time-resolved pump−probe spectroscopy experiments. Once the carriers reach the shifted band-edge states that are shifted by QSR, they can relax via radiative recombination, and the PL Stokes shift has significant contributions from QSR. As these contrasting models should have important impacts on our understanding of the energetics and carrier relaxation dynamics within SNCs, we emphasize the differences between the models here.

The biexciton interpretation is overviewed in Figure 7(a) and (b), which were adapted from Figure 6 in ref 54, using common labels appropriate for CdSe QDs.[95,96] The absorption of a high-energy photon generates hot carriers, an electron and hole in energetically excited states in the CB and VB. The $1S(e)-1S_L$ and $1S(e)-1S_U$ transitions experience an energetic shift with excitation referred to as the biexciton binding energy,

https://doi.org/10.1021/acsnano.4c09833
ACS Nano 2024, 18, 35104−35118

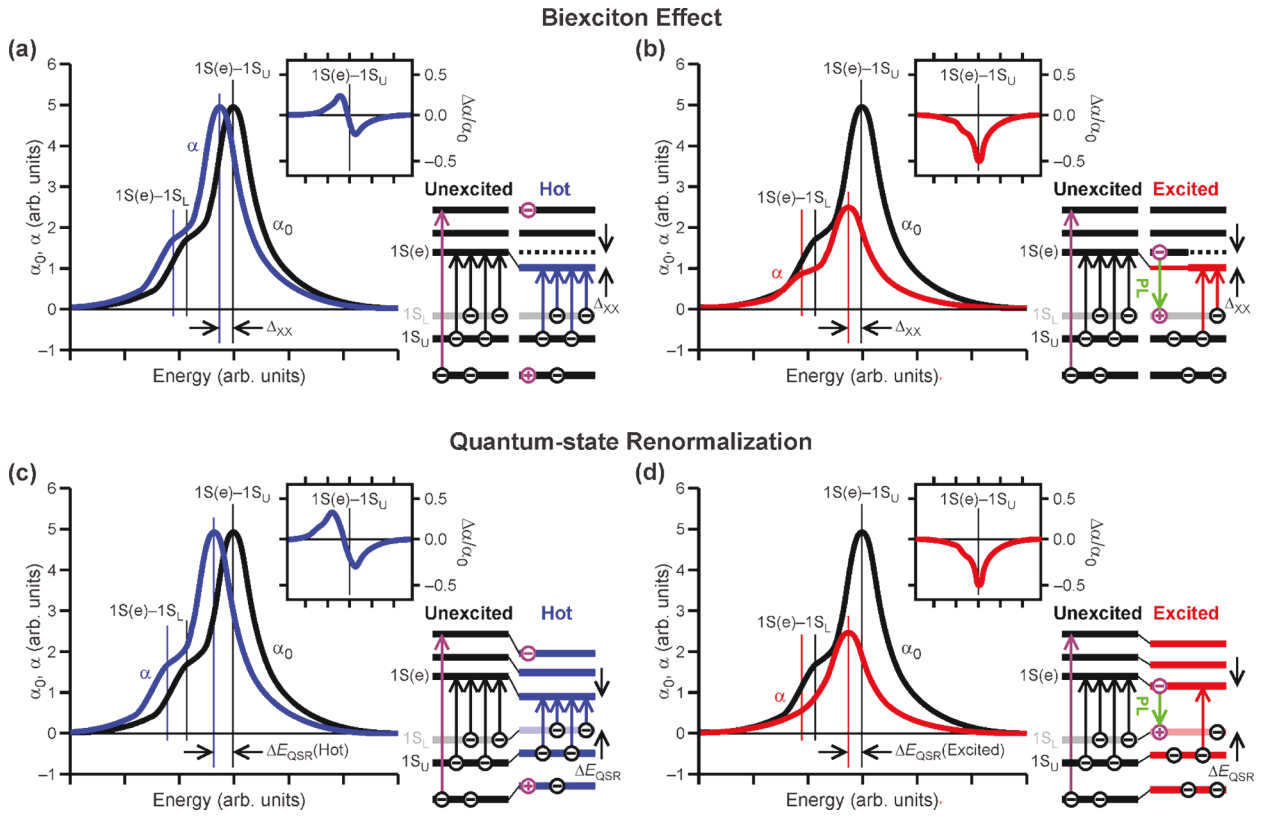

Figure 7. Schematic illustrations of the transient transitions of the band-edge states that result from excitation of a SNC. The state labels,[54] appropriate for CdSe QDs, are included for the lowest-energy electron state, 1S(e), and the two lowest-energy hole states, $1S_L$ and $1S_U$. The bright $1S(e)-1S_U$ and $1S(e)-1S_L$ absorptive transitions of the unexcited QD and the spectrum, α_0, are shown as black. The transitions and absorption spectra of the QD with hot carriers in highly excited states and with excited carriers in the band-edge states are shown as blue α and red α, respectively. The photoinduced changes probed in transient absorption experiments, $\Delta\alpha/\alpha_0$, are included in the insets. (a)−(b) Schematics overviewing the biexciton effect as presented by Klimov and illustrated in Figure 6 of ref 54. (a) Photoexcitation of an unexcited QD accesses transitions between the unperturbed quantum-confinement, black levels. The $1S(e)-1S_U$ and $1S(e)-1S_L$ transitions accessed by a second excitation are shifted by the biexciton binding energy, Δ_{XX}, and the $\Delta\alpha/\alpha_0$ spectrum has a derivative shape. (b) Once the electron and hole relax to the band-edge states, the electron in the 1S(e) state blocks one of the two $1S(e)-1S_L$ and one of the two $1S(e)-1S_U$ transitions. These transitions are shifted to lower energies in α as they access the biexciton state. The $\Delta\alpha/\alpha_0$ spectrum is dominated by the partially bleached $1S(e)-1S_U$ transition. Photoluminescence (PL) of room-temperature QDs in this model is primarily from the unperturbed $1S(e)-1S_L$ transition. (c)−(d) Schematics overviewing the QSR interpretation. Photoexcitation shifts each quantum-confinement state by unique energies that depend on the states occupied by carriers. (c) Photoexcitation to highly excited states results in a full bleach of the steady-state transitions, α_0, and the appearance of induced-absorption (IA) transitions between the shifted states, α. The $\Delta\alpha/\alpha_0$ spectrum appears with a derivative shape. (d) Once the carriers relax into the band-edge states, the $1S(e)-1S_L$ IA signal is fully bleached, and the $1S(e)-1S_U$ signal is partially bleached, and the $\Delta\alpha/\alpha_0$ spectrum is dominated by the bleach signal of the unperturbed $1S(e)-1S_U$ transition. The resultant PL is associated with the shifted $1S(e)-1S_L$ transition.

Δ_{XX}, black versus blue absorption line profiles, Figure 7(a). At short times, the amplitudes of these transitions are not affected by state filling, and the transient absorption signal near the band edge, $\Delta\alpha/\alpha_0$, appears with a first derivate profile, blue spectrum minus black spectrum. After intraband relaxation of the carriers is complete, the photoexcited electron and hole occupy the lowest-energy state, 1S(e) and $1S_L$, Figure 7(b). The single electron in the 1S(e) state bleaches by 50% the $1S(e)-1S_U$ transition, and there is induced-absorption associated with the biexciton-shifted state, red arrow. The single hole in the $1S_L$ state will bleach by 50% the $1S(e)-1S_L$ transition with the remaining transition energy shifted by Δ_{XX}. As a consequence, the $\Delta\alpha/\alpha_0$ transient signal at longer times contains less contributions from the biexciton state. The amplitude of the below-gap induced-absorption signal thus quickly decreases after excitation, and these time scales are oft associated with the biexciton lifetime for the QDs. Ultimately, the QD may undergo radiative recombination of the 1S(e) electron and the hole in the $1S_L$ state,[54] as indicated by the green arrow.

The energetics and transitions associated with QSR are overviewed in Figures 7(c) and (d) using the same QD system just described for biexcitons. The absorption of a high-energy photon generates hot carriers, and all of the quantum-confinement states experience unique ΔE_{QSR}, Figure 7(c). This state shifting gives rise to an energetic lowering of the absorptive transitions, blue arrows and blue α feature, and to $IA_{QSR}(E, t)$ signals in transient spectroscopy measurements. These signals appear on time scales that depend on the photoinducted changes in screening and the coupling with LO phonons via Fröhlich interactions. The energies of the states continue to shift by varying amounts as the carriers relax to the band-edge states. This represents the distinct difference of QSR from that of the biexciton model: It is the initial electron−hole pair that shifts the quantum-confinement states, not the second excitation associated with the probe laser

https://doi.org/10.1021/acsnano.4c09833
ACS Nano 2024, 18, 35104−35118

pulses. The dynamic QSR induced with photoexcitation of a SNC alters the energies of the quantum-confinement states and induces phonon coupling, and these likely contribute to the relaxation mechanisms of the carriers to the band-edge states.

Once the carriers relax into the band-edge states, each quantum-confinement state experiences a unique but constant ΔE_{QSR} as long as an excited charge carrier remains in the QD, indicated by red in Figure 7(d). At these long times, the $IA_{QSR}(E, t)$ signal associated with the shifted 1S(e)−$1S_L$ transition is fully are negated by the $BL_{Occ}(E, t)$ due to the electron and hole in the shifted 1S(e) and 1SL states. The $IA_{QSR}(E, t)$ signal associated with the 1S(e)−$1S_L$ transition is depleted by 50%, and the $BL_{QSR}(E, t)$ signal of the unperturbed 1S(e)−$1S_U$ transition dominates the transient $\Delta\alpha/\alpha_0$ signal at these long times, as shown in the inset in Figure 7(d). These below-gap $IA_{QSR}(E, t)$ signals tend to be absent or are greatly diminished even at short times for excitation energies close to the band edge, as shown in Figure 6(c) and (d), since the electrons are directly prepared in the lowest-energy state, and the $BL_{Occ}(E, t)$ contributions promptly negate the $IA_{QSR}(E, t)$ signals. The decay of the 1S(e)−$1S_U$ bleach signal, as well as all of the higher-energy IA and BL features associated with unoccupied states decay with the population of the electron and hole in each QD. Lastly, the radiative recombination of each electron−hole pair occurs from the carriers in the band-edge states shifted by ΔE_{QSR}, as depicted by the green arrow in Figure 7(d), and not from carriers in the unshifted states as inferred by the biexciton model, green arrow in Figure 7(b).

Fine Structure. Scrutiny of the Stokes shift of the PL(E) spectrum from the lowest-energy $Abs_{SS}(E)$ feature of SNCs provides further evidence for QSR induced by the photoexcitation of a single electron−hole pair. The Stokes shift, ΔE_S, is commonly attributed to the fine structure of the band-edge transitions.[54] The shapes and structures of the SNCs and electron−hole exchange interactions within them lift the degeneracy of the lowest-energy hole states, and there is fine structure present with contrasting oscillator strengths for transitions to the electron band-edge states.[54,95,96,113−119] Schematics illustrating these fine-structure energetics and contributions are included in Figure 8. Calculations indicate there are five different fine-structure transitions spanning an energy window <20 meV for wurtzite CdSe QDs with diameters of 6 nm.[113] The $Abs_{SS}(E)$ spectrum would have contributions from all of these transitions with those associated with the $|1^L\rangle$, $|1^U\rangle$, and $|0^U\rangle$ hole states dominant. After excitation, the electron and hole relax to the band-edge states, forming a quasi-equilibrium that results in a thermal distribution occupying those states. The concept often presented is that the lowest-energy hole states would be preferentially occupied, including the lowest-energy, optically dark $|2\rangle$ state, and that gives rise to the observed ΔE_S, as depicted in Figure 8(a). Due to the small energetic splitting of the fine-structure states the PL(E) spectrum of a room-temperature sample of the wurtzite CdSe QDs would likely have contributions from transitions associated with most if not all of the hole states, and only a small ΔE_S would be expected if this were the origin of the Stokes shift. Furthermore, it might be expected that the breadth of the room-temperature PL(E) spectrum would be narrower than the lowest-energy feature in the $Abs_{SS}(E)$ spectrum, especially for colloidal samples of

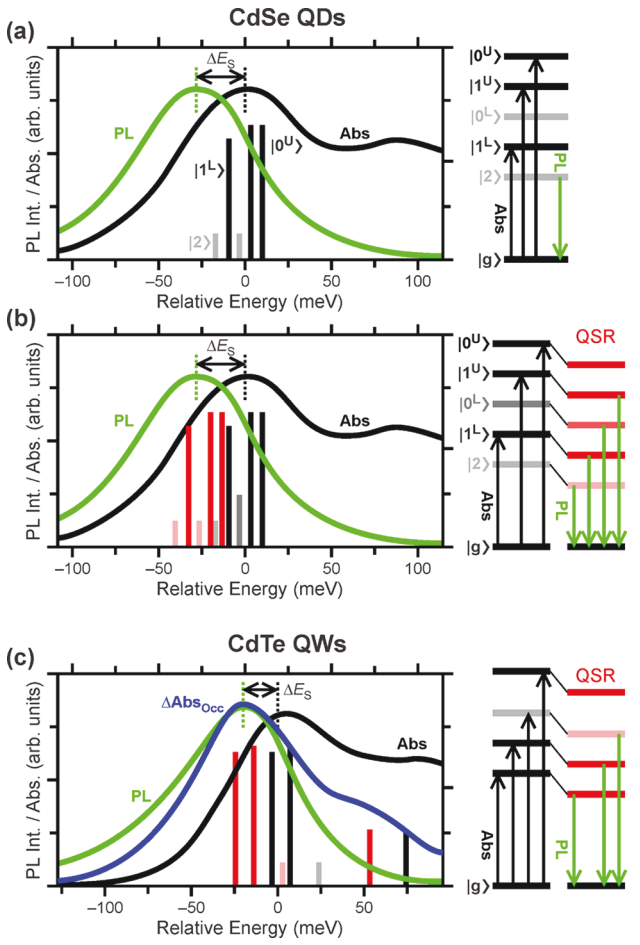

Figure 8. Schematics representing the contributions to the room-temperature Stokes shift for SNCs. The $Abs_{SS}(E)$ (black) and PL(E) (green) spectra are plotted versus the energy relative to the band-edge absorption feature with the Stokes shift, ΔE_S, indicated. (a) The spectral data for wurtzite CdSe QDs plotted with the calculated fine-structure transitions.[113] It is common to assume the ΔE_S is due to the unperturbed fine-structure of the hole states, even at room temperature. (b) The same data for CdSe QDs included in (a) with the calculated transitions (red lines) shifted by an assumed ΔE_{QSR} to account for the observed ΔE_S. (c) The spectral data for wurtzite CdTe QWs plotted with the calculated fine-structure calculations.[30,47] The calculated absorption lines were shifted by 20 meV (red lines) to reproduce the observed ΔE_S. The extracted $\Delta Abs_{QSR}(E, t)$ measured at t = 35 ps[30,47] overlaps very well the profile of the PL(E) spectrum.

SNCs with narrow size distributions. This narrowing of the PL(E) spectra, however, are not typically observed.

The QSR of the band-edge states at long times, as depicted in Figure 8(b), seems to be a more realistic explanation of the significant values of ΔE_S that are typically observed for room-temperature SNCs. Following photoexcitation of the carriers to high-energy states they undergo intraband relaxation to the band-edge states, which are shifted by QSR. The electrons will predominantly occupy the shifted 1S(e) state while the holes will occupy a thermal distribution of the shifted fine-structure states. Unless the unique ΔE_{QSR} values for all of the hole fine-structure states are drastically different, the PL(E) of a SNC will have a ΔE_S that is dominated by the ΔE_{QSR} of the 1S(e) and hole states with little difference between the breadths of the PL(E) spectrum and the lowest-energy band-edge absorption feature observed.

https://doi.org/10.1021/acsnano.4c09833
ACS Nano 2024, 18, 35104−35118

The steady-state spectroscopy and time-resolved TA data collected on CdTe QWs[30,31,47] provide strong additional evidence for the significant contributions of QSR in the room-temperature Stokes shift. Spectroscopic data collected for wurtzite CdTe QWs with a PL quantum yield of 0.2% are included in Figure 8(c) to illustrate this.[30,47] The dimensionality of the QWs results in the lowest-energy fine-structure hole states being optically bright,[95,96] and the calculated transitions for the CdTe QWs,[30,47] included in Figure 8(c), support these trends. The calculations indicate the two lowest-energy transition are optically bright, dominating the band-edge absorption.[30,47] It is necessary to shift these transitions by ∼20 meV to lower energies to best reproduce the PL(E) spectrum. Furthermore, The $\Delta Abs_{Occ}(E, t)$ spectra for t > 10 ps, after the carriers have relaxed into the band-edge states, blue spectrum in Figure 8(c), were extracted as described above.[30,47] The peaks of the $\Delta Abs_{Occ}(E, t)$ spectra at these long times are shifted by a constant energy that aligns very well with the peak of the PL(E) spectrum. These results indicate the QSR of the band-edge states contributes significantly to the Stokes shift, and the contributions of the fine structure to the Stokes shifts is likely small for most room-temperature SNCs.

SUMMARY AND FUTURE DIRECTIONS

In this Perspective, we highlight the concept of QSR within SNCs, or the independent shifting of the quantum-confinement states that depends on the states occupied by photoexcited charge carriers. QSR results in $BL_{QSR}(E, t)$ and $IA_{QSR}(E, t)$ features in time-resolved TA and 2DES data that energetically overlap the $BL_{Occ}(E, t)$ signals associated with the occupation of carriers in the different states. These QSR contributions in the time-resolved data appear on ultrashort time scales and remain as long as there are carriers in the SNCs. Thus, it is essential to account for QSR when evaluating TA and 2DES data to extract the time scales for intraband relaxation. The data collected on CdTe QWs indicate the intraband relaxation occurs on time scales that are ∼2× longer than the TA data itself would suggest. We propose that considering QSR when evaluating 2DES data and detailed comparisons of the temporal evolution of the cross peaks should provide details of these contributions.

The $IA_{QSR}(E, t)$ features present just below the band gap at short times in data collected with low-fluence photoexcitation to high-energy electron and hole states are akin to the BGR signals observed in many types of semiconductor materials. These features are short-lived since $BL_{Occ}(E, t)$ signals associated with carriers filling these states cancel the $IA_{QSR}(E, t)$ signals. These below-gap $IA_{QSR}(E, t)$ features are not observed when exciting at the band edge, as shown in Figure 6, since the carriers in these states promptly bleach these IA signals. We argue these $IA_{QSR}(E, t)$ features observed with low excitation fluences should not be considered biexciton features that would decay on time scales associated with Auger relaxation. The agreement between the long-time $\Delta AbsOcc(E, t)$ spectrum and the steady-state PL(E) spectrum measured for CdTe QWs provides strong evidence for that QSR provides a more accurate depiction of the interactions than the often implemented biexciton model.

Continued experimental and theoretical investigations undertaken on quantum-confined SNCs with varying dimensionalities and compositions that directly probe the energetics and dynamics of carriers with state specificity are essential for developing a better understanding of how photoexcitation perturbs the band structure and carrier dynamics within them. These agenda should include performing time-resolved TA spectroscopy as a function of excitation to different quantum-confinement states, identifying the contributions of separate electrons and holes versus bound excitons and the binding energies of the excitons, as well as characterizing the Fröhlich interactions on BGR and QSR. Improved models and excited-state calculations that include state-specific QSR contributions are needed to accurately separate and identify these contributions.

Lastly, the energetic consequences of BGR and QSR cause energetic perturbations of the quantum-confinement states, on the order of 10s to 100s of meV, but there are also structural changes incurred with photoexcitation and carrier recombination that may be of importance when implementing SNCs in devices and applications. Strategies that can minimize BGR, QSR, and carrier-phonon coupling within SNCs may prove particularly beneficial in device designs. The development of radially gradient multishell semiconductor QDs, for instance, has been shown to significantly suppress Auger relaxation.[120−126] It would be interesting to characterize how the smoothly varying crystal structure in gradient QDs impacts the photoexcited BGR and QSR within them.

AUTHOR INFORMATION

Corresponding Author

Richard A. Loomis − *Department of Chemistry and Institute of Materials Science and Engineering, Washington University in Saint Louis, Saint Louis, Missouri 63130, United States;* orcid.org/0000-0002-3172-6336; Email: loomis@wustl.edu

Authors

Jie Chen − *Department of Chemistry and Institute of Materials Science and Engineering, Washington University in Saint Louis, Saint Louis, Missouri 63130, United States;* orcid.org/0000-0002-6591-3412

Rena C. Kramer − *Department of Chemistry and Institute of Materials Science and Engineering, Washington University in Saint Louis, Saint Louis, Missouri 63130, United States*

Thomas R. Howell − *Department of Chemistry and Institute of Materials Science and Engineering, Washington University in Saint Louis, Saint Louis, Missouri 63130, United States;* orcid.org/0009-0005-0381-5269

Complete contact information is available at: https://pubs.acs.org/10.1021/acsnano.4c09833

Author Contributions

J.C., R.C.K., T.R.H., and R.A.L. contributed to the discussion of the content and revisions of the manuscript. R.A.L. conceived the idea. T.R.H. recorded the unpublished TA data on CdSe/ZnS QDs. All authors read and approved the final manuscript contents.

Notes

The authors declare no competing financial interest.

ACKNOWLEDGMENTS

This work was supported by the NSF under grant DMR-1905751. We thank P.J.B. and P.K. for providing the data published in ref 106 and included in Figure 6(e)−(h).

https://doi.org/10.1021/acsnano.4c09833
ACS Nano 2024, 18, 35104−35118

ABBREVIATIONS

SNC	Semiconductor nanocrystal
QSR	Quantum-state renormalization
PL	Photoluminescence
VB	Valence band
CB	Conduction band
EMA	Effective-mass approximation
BGR	Bandgap renormalization
1DPIB	One-dimensional particle-in-a-box
QP	Quantum platelet
Abs_{SS}	Steady-state absorption spectrum
TA	Transient absorption
E_{exc}	Excitation energy
BL	Bleach
BL_{QSR}	Bleach transitions associated with QSR
BL_{Occ}	Bleach transitions associated with carriers occupying a state
SE_{Occ}	Stimulated emission associated with carriers occupying a state
IA	Induced-absorption
IA_{QSR}	Induced-absorption transitions associated with QSR
ΔAbs_{QSR}	Spectral contributions from QSR
ΔAbs_{Occ}	Spectrum containing all BL_{Occ} contributions
ΔAbs_{TA}	Transient absorption signals
ΔE_{QSR}	Energetic shift of a state attributed to QSR
QD	Quantum dot
TMDs	Transition metal dichalcogenides
1ML	Single-monolayer
NCs	Nanocrystals
QW	Quantum wire
2DES	Two-dimensional electronic spectroscopy
E_1	Excitation energy in a 2DES experiment
E_3	Emission or detection energy in a 2DES experiment
Δ_{XX}	Biexciton binding energy
ESA	Excited-state absorption

REFERENCES

(1) Leschkies, K. S.; Divakar, R.; Basu, J.; Enache-Pommer, E.; Boercker, J. E.; Carter, C. B.; Kortshagen, U. R.; Norris, D. J.; Aydil, E. S. Photosensitization of ZnO nanowires with CdSe quantum dots for photovoltaic devices. *Nano Lett.* **2007**, *7*, 1793−1798.

(2) Kapon, E.; Simhony, S.; Bhat, R.; Hwang, D. M. Single quantum wire semiconductor lasers. *Appl. Phys. Lett.* **1989**, *55*, 2715−2717.

(3) Vaillancourt, J.; Vasinajindakaw, P.; Lu, X. A high operating temperature (hot) middle wave infrared (MWIR) quantum-dot photodetector. *Opt. Photon. Lett.* **2011**, *04*, 57−61.

(4) Howarth, M.; Liu, W.; Puthenveetil, S.; Zheng, Y.; Marshall, L. F.; Schmidt, M. M.; Wittrup, K. D.; Bawendi, M. G.; Ting, A. Y. Monovalent, reduced-size quantum dots for imaging receptors on living cells. *Nat. Methods* **2008**, *5*, 397−399.

(5) Law, M.; Greene, L. E.; Johnson, J. C.; Saykally, R.; Yang, P. Nanowire dye-sensitized solar cells. *Nature* **2005**, *4*, 455−459.

(6) Dingle, R. Confined carrier quantum states in ultrathin semiconductor heterostructures. *Festkoerperprobleme* **1975**, *15*, 21−48.

(7) Yoffe, A. D. Low-dimensional systems: quantum size effects and electronic properties of semiconductor microcrystallites (zero-dimensional systems) and some quasi-two-dimensional systems. *Adv. Phys.* **1993**, *42*, 173−266.

(8) Adamowski, J. Formation of Fröhlich bipolarons. *Phys. Rev. B* **1989**, *39*, 3649−3652.

(9) Kelley, A. M. Electron-phonon coupling in CdSe nanocrystals. *J. Phys. Chem. Lett.* **2010**, *1*, 1296−1300.

(10) Kelley, A. M. Electron-phonon coupling in CdSe nanocrystals from an atomistic phonon model. *ACS Nano* **2011**, *5*, 5254−5262.

(11) Kelley, A. M.; Dai, Q.; Jiang, Z.-j.; Baker, J. A.; Kelley, D. F. Resonance Raman spectra of wurtzite and zincblende CdSe nanocrystals. *Chem. Phys.* **2013**, *422*, 272−276.

(12) Lin, C.; Gong, K.; Kelley, D. F.; Kelley, A. M. Electron-phonon coupling in CdSe/CdS core/shell quantum dots. *ACS Nano* **2015**, *9*, 8131−8141.

(13) Park, Y.; Limmer, D. T. Renormalization of excitonic properties by polar phonons. *J. Chem. Phys.* **2022**, *157*, 104116.

(14) Sagar, D. M.; Cooney, R. R.; Sewall, S. L.; Dias, E. A.; Barsan, M. M.; Butler, I. S.; Kambhampati, P. Size dependent, state-resolved studies of exciton-phonon couplings in strongly confined semiconductor quantum dots. *Phys. Rev. B* **2008**, *77*, 235321.

(15) Sagar, D. M.; Cooney, R. R.; Sewall, S. L.; Kambhampati, P. State-resolved exciton-phonon couplings in CdSe semiconductor quantum dots. *J. Phys. Chem. C* **2008**, *112*, 9124−9127.

(16) Plekhanov, V. G. Chapter 6: Exciton-phonon interaction. In *Semiconductors and Semimetals*; Plekhanov, V. G., Ed.; Elsevier: 2001; Vol. *68*, pp 135−180.

(17) Bawendi, M. G.; Wilson, W. L.; Rothberg, L.; Carroll, P. J.; Jedju, T. M.; Steigerwald, M. L.; Brus, L. E. Electronic structure and photoexcited-carrier dynamics in nanometer-size CdSe clusters. *Phys. Rev. Lett.* **1990**, *65*, 1623−1626.

(18) Glässl, M.; Vagov, A.; Lüker, S.; Reiter, D. E.; Croitoru, M. D.; Machnikowski, P.; Axt, V. M.; Kuhn, T. Long-time dynamics and stationary nonequilibrium of an optically driven strongly confined quantum dot coupled to phonons. *Phys. Rev. B* **2011**, *84*, 195311.

(19) Boldt, K. Raman spectroscopy of colloidal semiconductor nanocrystals. *Nano Futures* **2022**, *6*, 012003.

(20) Kleinman, D. A.; Miller, R. C. Band-gap renormalization in semiconductor quantum wells containing carriers. *Phys. Rev. B* **1985**, *32*, 2266−2272.

(21) Bennett, C. R.; Güven, K.; Tanatar, B. Confined-phonon effects in the band-gap renormalization of semiconductor quantum wires. *Phys. Rev. B* **1998**, *57*, 3994−3999.

(22) Spataru, C. D.; Benedict, L. X.; Louie, S. G. *Ab initio* calculation of band-gap renormalization in highly excited GaAs. *Phys. Rev. B* **2004**, *69*, 205204.

(23) Vashishta, P.; Kalia, R. K. Universal behavior of exchange-correlation energy in electron-hole liquid. *Phys. Rev. B* **1982**, *25*, 6492−6495.

(24) Swoboda, H. E.; Sence, M.; Majumder, F. A.; Rinker, M.; Bigot, J. Y.; Grun, J. B.; Klingshirn, C. Properties of the electron-hole plasma in II-VI compounds as a function of temperature. *Phys. Rev. B* **1989**, *39*, 11019−11027.

(25) Cingolani, R.; Rinaldi, R.; Ferrara, M.; La Rocca, G. C.; Lage, H.; Heitmann, D.; Ploog, K.; Kalt, H. Band-gap renormalization in quantum wires. *Phys. Rev. B* **1993**, *48*, 14331−14337.

(26) Heitz, R.; Guffarth, F.; Mukhametzhanov, I.; Grundmann, M.; Madhukar, A.; Bimberg, D. Many-body effects on the optical spectra of InAs/GaAs quantum dots. *Phys. Rev. B* **2000**, *62*, 16881−16885.

(27) Güven, K.; Tanatar, B.; Bennett, C. R. Band-gap renormalization in quantum wire systems: dynamical correlations and multisubband effects. *J. Phys.-Condens. Mater.* **2000**, *12*, 2031−2042.

(28) Nagai, T.; Inagaki, T. J.; Kanemitsu, Y. Band-gap renormalization in highly excited GaN. *Appl. Phys. Lett.* **2004**, *84*, 1284−1286.

(29) Cunningham, P. D.; Hanbicki, A. T.; McCreary, K. M.; Jonker, B. T. Photoinduced bandgap renormalization and exciton binding energy reduction in WS_2. *ACS Nano* **2017**, *11*, 12601−12608.

(30) Sanderson, W. M.; Schrier, J.; Wang, F.; Buhro, W. E.; Loomis, R. A. Intraband relaxation dynamics of charge carriers within CdTe quantum wires. *J. Phys. Chem. Lett.* **2020**, *11*, 4901−4910.

(31) Chen, J.; Sanderson, W. M.; Loomis, R. A. Dynamic quantum-state renormalization and effects of competing pathways on carrier relaxation in semiconductor nanoparticles. *J. Phys. Chem. C* **2023**, *127*, 20082−20093.

(32) Klimov, V. I.; McBranch, D. W. Femtosecond 1*P*-to-1*S* electron relaxation in strongly confined semiconductor nanocrystals. *Phys. Rev. Lett.* **1998**, *80*, 4028−4031.

https://doi.org/10.1021/acsnano.4c09833
ACS Nano 2024, 18, 35104−35118

(33) Klimov, V. I.; McBranch, D. W.; Leatherdale, C. A.; Bawendi, M. G. Electron and hole relaxation pathways in semiconductor quantum dots. *Phys. Rev. B* **1999**, *60*, 13740−13749.
(34) Klimov, V. I.; Mikhailovsky, A. A.; McBranch, D. W.; Leatherdale, C. A.; Bawendi, M. G. Mechanisms for intraband energy relaxation in semiconductor quantum dots: The role of electron-hole interactions. *Phys. Rev. B* **2000**, *61*, R13349−R13352.
(35) Sewall, S. L.; Cooney, R. R.; Anderson, K. E. H.; Dias, E. A.; Kambhampati, P. State-to-state exciton dynamics in semiconductor quantum dots. *Phys. Rev. B* **2006**, *74*, 235328.
(36) Cooney, R. R.; Sewall, S. L.; Dias, E. A.; Sagar, D. M.; Anderson, K. E. H.; Kambhampati, P. Unified picture of electron and hole relaxation pathways in semiconductor quantum dots. *Phys. Rev. B* **2007**, *75*, 245311.
(37) Jiang, Z.-J.; Kelley, D. F. Hot and relaxed electron transfer from the CdSe core and core/shell nanorods. *J. Phys. Chem. C* **2011**, *115*, 4594−4602.
(38) Kambhampati, P. Hot exciton relaxation dynamics in semiconductor quantum dots: Radiationless transitions on the nanoscale. *J. Phys. Chem. C* **2011**, *115*, 22089−22109.
(39) Wheeler, D. A.; Zhang, J. Z. Exciton dynamics in semiconductor nanocrystals. *Adv. Mater.* **2013**, *25*, 2878−2896.
(40) Kennehan, E. R.; Doucette, G. S.; Marshall, A. R.; Grieco, C.; Munson, K. T.; Beard, M. C.; Asbury, J. B. Electron-phonon coupling and resonant relaxation from 1D and 1P states in PbS quantum dots. *ACS Nano* **2018**, *12*, 6263−6272.
(41) Burda, C.; Link, S.; Green, T. C.; El-Sayed, M. A. New transient absorption observed in the spectrum of colloidal CdSe nanoparticles pumped with high-power femtosecond pulses. *J. Phys. Chem. B* **1999**, *103*, 10775−10780.
(42) Carey, C. R.; Yu, Y.; Kuno, M.; Hartland, G. V. Ultrafast transient absorption measurements of charge carrier dynamics in single II-VI nanowires. *J. Phys. Chem. C* **2009**, *113*, 19077−19081.
(43) Lo, S. S.; Major, T. A.; Petchsang, N.; Huang, L. B.; Kuno, M.; Hartland, G. V. CdTe nanowires studied by transient absorption microscopy. *EPJ. Web of Conferences* **2013**, *41*, 04032.
(44) Robel, I.; Bunker, B. A.; Kamat, P. V.; Kuno, M. Exciton recombination dynamics in CdSe nanowires: Bimolecular to three-carrier Auger kinetics. *Nano Lett.* **2006**, *6*, 1344−1349.
(45) Mooney, J.; Krause, M. M.; Kambhampati, P. Connecting the dots: The kinetics and thermodynamics of hot, cold, and surface-trapped excitons in semiconductor nanocrystals. *J. Phys. Chem. C* **2014**, *118*, 7730−7739.
(46) McArthur, E. A.; Morris-Cohen, A. J.; Knowles, K. E.; Weiss, E. A. Charge carrier resolved relaxation of the first excitonic state in CdSe quantum dots probed with near-infrared transient absorption spectroscopy. *J. Phys. Chem. B* **2010**, *114*, 14514−14520.
(47) Sanderson, W. M.; Schrier, J.; Loomis, R. A. Photo-induced state shifting in 1D semiconductor quantum wires. *J. Phys. Chem. C* **2020**, *124*, 16702−16713.
(48) Morgan, D. P.; Kelley, D. F. What does the transient absorption spectrum of CdSe quantum dots measure? *J. Phys. Chem. C* **2020**, *124*, 8448−8455.
(49) Morgan, D. P.; Maddux, C. J. A.; Kelley, D. F. Transient absorption spectroscopy of CdSe nanoplatelets. *J. Phys. Chem. C* **2018**, *122*, 23772−23779.
(50) Yan, Y.; Chen, G.; Van Patten, P. G. Ultrafast exciton dynamics in CdTe nanocrystals and core/shell CdTe/CdS nanocrystals. *J. Phys. Chem. C* **2011**, *115*, 22717−22728.
(51) Zhang, C.; Xu, J.; Zhu, T.; Zhang, F.; Tan, Z.; Schiff, S. J.; Su, H.; Gao, S.; Wang, A. Y. Quantum efficiency of stimulated emission in colloidal semiconductor nanocrystal quantum dots. *Phys. Rev. B* **2009**, *80*, 035333.
(52) Klimov, V.; Hunsche, S.; Kurz, H. Biexciton effects in femtosecond nonlinear transmission of semiconductor quantum dots. *Phys. Rev. B* **1994**, *50*, 8110−8113.
(53) Klimov, V. I. Optical nonlinearities and ultrafast carrier dynamics in semiconductor nanocrystals. *J. Phys. Chem. B* **2000**, *104*, 6112−6123.
(54) Klimov, V. I. Properties of multiexcitons in semiconductor nanocrystals. *Annu. Rev. Phys. Chem.* **2007**, *58*, 635−673.
(55) Sewall, S. L.; Cooney, R. R.; Anderson, K. E. H.; Dias, E. A.; Sagar, D. M.; Kambhampati, P. State-resolved studies of biexcitons and surface trapping dynamics in semiconductor quantum dots. *J. Chem. Phys.* **2008**, *129*, 084701.
(56) Sewall, S. L.; Franceschetti, A.; Cooney, R. R.; Zunger, A.; Kambhampati, P. Direct obervation of the structure of band-edge biexcitons in colloidal semiconductor CdSe quantum dots. *Phys. Rev. B* **2009**, *80*, No. 081310.
(57) Sewall, S. L.; Cooney, R. R.; Dias, E. A.; Tyagi, P.; Kambhampati, P. State-resolved observation in real time of the structural dynamics of multiexcitons in semiconductor nanocrystals. *Phys. Rev. B* **2011**, *84*, 235304.
(58) Saari, J. I.; Dias, E. A.; Reifsnyder, D.; Krause, M. M.; Walsh, B. R.; Murray, C. B.; Kambhampati, P. Ultrafast electron trapping at the surface of semiconductor nanocrystals: Excitonic and biexcitonic processes. *J. Phys. Chem. B* **2013**, *117*, 4412−4421.
(59) Seiler, H.; Palato, S.; Sonnichsen, C.; Baker, H.; Kambhampati, P. Seeing multiexcitons through sample inhomogeneity: Band-edge biexciton structure in CdSe nanocrystals revealed by two-dimensional electronic spectroscopy. *Nano Lett.* **2018**, *18*, 2999−3006.
(60) Palato, S.; Seiler, H.; Baker, H.; Sonnichsen, C.; Brosseau, P.; Kambhampati, P. Investigating the electronic structure of confined multiexcitons with nonlinear spectroscopies. *J. Chem. Phys.* **2020**, *152*, 104710.
(61) Turner, D. B.; Hassan, Y.; Scholes, G. D. Exciton superposition states in CdSe nanocrystals measured using broadband two-dimensional electronic spectroscopy. *Nano Lett.* **2012**, *12*, 880−886.
(62) Griffin, G. B.; Ithurria, S.; Dolzhnikov, D. S.; Linkin, A.; Talapin, D. V.; Engel, G. S. Two-dimensional electronic spectroscopy of CdSe nanoparticles at very low pulse power. *J. Chem. Phys.* **2013**, *138*, 014705.
(63) Hu, Y. Z.; Koch, S. W.; Lindberg, M.; Peyghambarian, N.; Pollock, E. L.; Abraham, F. F. Biexcitons in semiconductor quantum dots. *Phys. Rev. Lett.* **1990**, *64*, 1805−1807.
(64) Voss, T.; Rückmann, I.; Gutowski, J.; Axt, V. M.; Kuhn, T. Coherent control of the exciton and exciton-biexciton transitions in the generation of nonlinear wave-mixing signals in a semiconductor quantum well. *Phys. Rev. B* **2006**, *73*, 115311.
(65) Kambhampati, P. Multiexcitons in semiconductor nanocrystals: A platform for optoelectronics at high carrier concentration. *J. Phys. Chem. Lett.* **2012**, *3*, 1182−1190.
(66) Pogna, E. A. A.; Marsili, M.; De Fazio, D.; Dal Conte, S.; Manzoni, C.; Sangalli, D.; Yoon, D.; Lombardo, A.; Ferrari, A. C.; Marini, A.; Cerullo, G.; Prezzi, D. Photo-induced bandgap renormalization governs the ultrafast response of single-layer MoS_2. *ACS Nano* **2016**, *10*, 1182−1188.
(67) Lin, Y.; Chan, Y.-h.; Lee, W.; Lu, L.-S.; Li, Z.; Chang, W.-H.; Shih, C.-K.; Kaindl, R. A.; Louie, S. G.; Lanzara, A. *Exciton-driven ultrafast enhancement of quasiparticle bandgap and effective mass in monolayer MoS_2*. Conference on Lasers and Electro-Optics, San Jose, California, May 15, 2022; Optica Publishing Group: San Jose, CA, 2022; p FTu4B.1.
(68) Lin, Y.; Chan, Y.-h.; Lee, W.; Lu, L.-S.; Li, Z.; Chang, W.-H.; Shih, C.-K.; Kaindl, R. A.; Louie, S. G.; Lanzara, A. Exciton-driven renormalization of quasiparticle band structure in monolayer MoS_2. *Phys. Rev. B* **2022**, *106*, L081117.
(69) Ugeda, M. M.; Bradley, A. J.; Shi, S.-F.; da Jornada, F. H.; Zhang, Y.; Qiu, D. Y.; Ruan, W.; Mo, S.-K.; Hussain, Z.; Shen, Z.-X.; Wang, F.; Louie, S. G.; Crommie, M. F. Giant bandgap renormalization and excitonic effects in a monolayer transition metal dichalcogenide semiconductor. *Nat. Mater.* **2014**, *13*, 1091−1095.
(70) Shukla, A.; Kaur, G.; Babu, K. J.; Ghorai, N.; Goswami, T.; Kaur, A.; Ghosh, H. N. Effect of confinement on the exciton and biexciton dynamics in perovskite 2D-nanosheets and 3D-nanocrystals. *J. Phys. Chem. Lett.* **2020**, *11*, 6344−6352.

https://doi.org/10.1021/acsnano.4c09833
ACS Nano 2024, 18, 35104−35118

(71) Laboratory, N. R. E. Best Research-Cell Efficiency Chart. https://www.nrel.gov/pv/cell-efficiency.html (Last accessed: September 4, 2024).
(72) George, J.; Joseph, A. P.; Balachandran, M. Perovskites: Emergence of highly efficient third-generation solar cells. *Int. J. Energy Res.* **2022**, *46*, 21856−21883.
(73) Price, M. B.; Butkus, J.; Jellicoe, T. C.; Sadhanala, A.; Briane, A.; Halpert, J. E.; Broch, K.; Hodgkiss, J. M.; Friend, R. H.; Deschler, F. Hot-carrier cooling and photoinduced refractive index changes in organic-inorganic lead halide perovskites. *Nat. Commun.* **2015**, *6*, 8420.
(74) Anand, B.; Sampat, S.; Danilov, E. O.; Peng, W.; Rupich, S. M.; Chabal, Y. J.; Gartstein, Y. N.; Malko, A. V. Broadband transient absorption study of photoexcitations in lead halide perovskites: Towards a multiband picture. *Phys. Rev. B* **2016**, *93*, 161205.
(75) Butkus, J.; Vashishtha, P.; Chen, K.; Gallaher, J. K.; Prasad, S. K. K.; Metin, D. Z.; Laufersky, G.; Gaston, N.; Halpert, J. E.; Hodgkiss, J. M. The evolution of quantum confinement in $CsPbBr_3$ perovskite nanocrystals. *Chem. Mater.* **2017**, *29*, 3644−3652.
(76) Telfah, H.; Jamhawi, A.; Teunis, M. B.; Sardar, R.; Liu, J. Ultrafast exciton dynamics in shape-controlled methylammonium lead bromide perovskite nanostructures: Effect of quantum confinement on charge carrier recombination. *J. Phys. Chem. C* **2017**, *121*, 28556−28565.
(77) Ghosh, T.; Aharon, S.; Shpatz, A.; Etgar, L.; Ruhman, S. Reflectivity effects on pump-probe spectra of lead halide perovskites: Comparing thin films versus nanocrystals. *ACS Nano* **2018**, *12*, 5719−5725.
(78) Tamming, R. R.; Butkus, J.; Price, M. B.; Vashishtha, P.; Prasad, S. K. K.; Halpert, J. E.; Chen, K.; Hodgkiss, J. M. Ultrafast spectrally resolved photoinduced complex refractive index changes in $CsPbBr_3$ perovskites. *ACS Photonics* **2019**, *6*, 345−350.
(79) Narra, S.; Lin, C.-Y.; Seetharaman, A.; Jokar, E.; Diau, E. W.-G. Femtosecond exciton and carrier relaxation dynamics of two-dimensional (2D) and quasi-2D tin perovskites. *J. Phys. Chem. Lett.* **2021**, *12*, 12292−12299.
(80) Yan, J.; Jiang, T.; Liu, Q.; Xiao, Z.; Zhang, W.; Zhou, H.; Wu, G.; Chen, Z. Giant band-gap renormalization and morphology-tunable defect-assisted carrier recombination in $CsPbBr_3$ microstructures. *ACS Photonics* **2023**, *10*, 3976−3984.
(81) Ravali, V.; Ghosh, T. Charge carrier dynamics and transient spectral evolutions in lead halide perovskites. *ChemComm* **2023**, *59*, 13939−13950.
(82) Wang, L.; Nughays, R.; Yin, J.; Shih, C.-H.; Guo, T.-F.; Mohammed, O. F.; Chergui, M. Band gap renormalization at different symmetry points in perovskites. *ACS Photonics* **2024**, *11*, 2273−2281.
(83) Soetan, N.; Puretzky, A.; Reid, K.; Boulesbaa, A.; Zarick, H. F.; Hunt, A.; Rose, O.; Rosenthal, S.; Geohegan, D. B.; Bardhan, R. Ultrafast spectral dynamics of $CsPb(Br_xCl_{1-x})_3$ mixed-halide nanocrystals. *ACS Photonics* **2018**, *5*, 3575−3583.
(84) Yumoto, G.; Tahara, H.; Kawawaki, T.; Saruyama, M.; Sato, R.; Teranishi, T.; Kanemitsu, Y. Hot biexciton effect on optical gain in $CsPbI_3$ perovskite nanocrystals. *J. Phys. Chem. Lett.* **2018**, *9*, 2222−2228.
(85) Yumoto, G.; Kanemitsu, Y. Biexciton dynamics in halide perovskite nanocrystals. *Phys. Chem. Chem. Phys.* **2022**, *24*, 22405−22425.
(86) Yu, B.; Zhang, C.; Chen, L.; Qin, Z.; Huang, X.; Wang, X.; Xiao, M. Ultrafast dynamics of photoexcited carriers in perovskite semiconductor nanocrystals. *Nanophotonics* **2021**, *10*, 1943−1965.
(87) Shukla, A.; Kaur, G.; Babu, K. J.; Ghosh, H. N. Spectroscopic investigation of structural perturbations in $CsPbCl_3$ perovskite nanocrystals: Temperature- and excitation-energy-dependent study. *ACS Photonics* **2023**, *10*, 1906−1915.
(88) Poonia, A. K.; Yadav, P.; Mondal, B.; Mandal, D.; Taank, P.; Shrivastava, M.; Nag, A.; Agarwal, A.; Adarsh, K. V. Room-temperature electron-hole condensation in direct-band-gap semiconductor nanocrystals. *Phys. Rev. Applied* **2023**, *20*, L021002.
(89) Maurya, N. C.; Karmakar, R.; Yadav, R. K.; Taank, P.; Bera, S. K.; Mondal, A.; Mandal, D.; Shrivastava, M.; Hasan, M. N.; Maji, T. K.; Karmakar, D.; Adarsh, K. V. Exciton many-body interactions and charge transfer in $CsPbBr_3$/graphene derivatives. *Phys. Rev. B* **2023**, *108*, 155417.
(90) Sanderson, W. M.; Wang, F.; Buhro, W. E.; Loomis, R. A. Long-lived 1D excitons in bright CdTe quantum wires. *J. Phys. Chem. C* **2019**, *123*, 3144−3151.
(91) Wayman, V. L.; Morrison, P. J.; Wang, F.; Tang, R.; Buhro, W. E.; Loomis, R. A. Bound 1D excitons in single CdSe quantum wires. *J. Phys. Chem. Lett.* **2012**, *3*, 2627−2632.
(92) Emin, D. *Polarons*; Cambridge University Press: New York, 2013; p 227.
(93) Khosla, M.; Rao, S.; Gupta, S. Polarons explain luminescence behavior of colloidal quantum dots at low temperature. *Sci. Rep.* **2018**, *8*, 8385.
(94) Maslov, A. Y.; Proshina, O. V. Interface phonons and polaron states in quantum nanostructures. In *Phonons in Low Dimensional Structures*; Stavrou, V., Ed.; IntechOpen: London, 2018; pp 3−17.
(95) Efros, A. L.; Rosen, M.; Kuno, M.; Nirmal, M.; Norris, D. J.; Bawendi, M. Band-edge exciton in quantum dots of semiconductors with a degenerate valence band: Dark and bright exciton states. *Phys. Rev. B* **1996**, *54*, 4843−4856.
(96) Zhao, Q.; Graf, P. A.; Jones, W. B.; Franceschetti, A.; Li, J.; Wang; Kim, K. Shape dependence of band-edge exciton fine structure in CdSe nanocrystals. *Nano Lett.* **2007**, *7*, 3274−3280.
(97) Kramer, R. C.; Howell, T. R.; Loomis, R. A. Contributions of QSR in colloidal semiconductor nanocrystals with contrasting dimensionalities. Unpublished data, 2024.
(98) Collini, E. 2D electronic spectroscopic techniques for quantum technology applications. *J. Phys. Chem. C* **2021**, *125*, 13096−13108.
(99) Cassette, E.; Dean, J. C.; Scholes, G. D. Two-dimensional visible spectroscopy for studying colloidal semiconductor nanocrystals. *Small* **2016**, *12*, 2234−2244.
(100) Caram, J. R.; Zheng, H.; Dahlberg, P. D.; Rolczynski, B. S.; Griffin, G. B.; Dolzhnikov, D. S.; Talapin, D. V.; Engel, G. S. Exploring size and state dynamics in CdSe quantum dots using two-dimensional electronic spectroscopy. *J. Chem. Phys.* **2014**, *140*, 084701.
(101) Cassette, E.; Pensack, R. D.; Mahler, B.; Scholes, G. D. Room-temperature exciton coherence and dephasing in two-dimensional nanostructures. *Nat. Commun.* **2015**, *6*, 6086.
(102) Caram, J. R.; Zheng, H.; Dahlberg, P. D.; Rolczynski, B. S.; Griffin, G. B.; Fidler, A. F.; Dolzhnikov, D. S.; Talapin, D. V.; Engel, G. S. Persistent interexcitonic quantum coherence in CdSe quantum dots. *J. Phys. Chem. Lett.* **2014**, *5*, 196−204.
(103) Seiler, H.; Palato, S.; Kambhampati, P. Investigating exciton structure and dynamics in colloidal CdSe quantum dots with two-dimensional electronic spectroscopy. *J. Chem. Phys.* **2018**, *149*, 074702.
(104) Stoll, T.; Branchi, F.; Réhault, J.; Scotognella, F.; Tassone, F.; Kriegel, I.; Cerullo, G. Two-dimensional electronic spectroscopy unravels sub-100 fs electron and hole relaxation dynamics in Cd-chalcogenide nanostructures. *J. Phys. Chem. Lett.* **2017**, *8*, 2285−2290.
(105) Karki, K. J.; Widom, J. R.; Seibt, J.; Moody, I.; Lonergan, M. C.; Pullerits, T.; Marcus, A. H. Coherent two-dimensional photocurrent spectroscopy in a PbS quantum dot photocell. *Nat. Commun.* **2014**, *5*, 5869.
(106) Brosseau, P. J.; Geuchies, J. J.; Jasrasaria, D.; Houtepen, A. J.; Rabani, E.; Kambhampati, P. Ultrafast hole relaxation dynamics in quantum dots revealed by two-dimensional electronic spectroscopy. *Commun. Phys.* **2023**, *6*, 48.
(107) Grun, J. B.; Honerlage, B.; Levy, R. Excitons. In *Excitons*; Rashba, E. I., Sturge, M. D., Eds.; North-Holland Pub. Co.: Amsterdam, The Netherlands, 1982; p 459.
(108) Kleinman, D. A. Binding energy of biexcitons and bound excitons in quantum wells. *Phys. Rev. B* **1983**, *28*, 871−879.

https://doi.org/10.1021/acsnano.4c09833
ACS Nano 2024, 18, 35104−35118

(109) Hönerlage, B.; Lévy, R.; Grun, J. B.; Klingshirn, C.; Bohnert, K. The dispersion of excitons, polaritons and biexcitons in direct-gap semiconductors. *Phys. Rep.* **1985**, *124*, 161−253.
(110) Banyai, L.; Hu, Y. Z.; Lindberg, M.; Koch, S. W. Third-order optical nonlinearities in semiconductor microstructures. *Phys. Rev. B* **1988**, *38*, 8142−8153.
(111) Bressanini, D.; Mella, M.; Morosi, G. Stability of four-body systems in three and two dimensions: A theoretical and quantum Monte Carlo study of biexciton molecules. *Phys. Rev. A* **1998**, *57*, 4956−4959.
(112) Vonk, S. J. W.; Heemskerk, B. A. J.; Keitel, R. C.; Hinterding, S. O. M.; Geuchies, J. J.; Houtepen, A. J.; Rabouw, F. T. Biexciton binding energy and line width of single quantum dots at room temperature. *Nano Lett.* **2021**, *21*, 5760−5766.
(113) Norris, D. J.; Efros, A. L.; Rosen, M.; Bawendi, M. G. Size dependence of exciton fine structure in CdSe quantum dots. *Phys. Rev. B* **1996**, *53*, 16347−16354.
(114) Efros, A. L.; Rosen, M. The electronic structure of semiconductor nanocrystals. *Annu. Rev. Mater. Sci.* **2000**, *30*, 475−521.
(115) Crooker, S. A.; Barrick, T.; Hollingsworth, J. A.; Klimov, V. I. Multiple temperature regimes of radiative decay in CdSe nanocrystal quantum dots: Intrinsic limits to the dark-exciton lifetime. *Appl. Phys. Lett.* **2003**, *82*, 2793−2795.
(116) de Mello Donegá, C.; Bode, M.; Meijerink, A. Size- and temperature-dependence of exciton lIfetimes in CdSe quantum dots. *Phys. Rev. B* **2006**, *74*, 085320.
(117) Hoang, T. B.; Titova, L. V.; Jackson, H. E.; Smith, L. M.; Yarrison-Rice, J. M.; Lensch, J. L.; Lauhon, L. J. Temperature dependent photoluminescence of single CdS nanowires. *Appl. Phys. Lett.* **2006**, *89*, 123123.
(118) Furis, M.; Barrick, T.; Robbins, P.; Crooker, S. A.; Petruska, M.; Klimov, V.; Efros, A. L. Exciton spin states in nanocrystal quantum dots revealed by spin-polarized resonant photoluminescence and Raman spectroscopy. *Int. J. Mod. Phys. B* **2004**, *18*, 3769−3774.
(119) Furis, M.; Htoon, H.; Petruska, M. A.; Klimov, V. I.; Barrick, T.; Crooker, S. A. Bright-exciton fine structure and anisotropic exchange in CdSe nanocrystal quantum dots. *Phys. Rev. B* **2006**, *73*, 241313.
(120) Cragg, G. E.; Efros, A. L. Suppression of Auger processes in confined structures. *Nano Lett.* **2010**, *10*, 313−317.
(121) Climente, J. I.; Movilla, J. L.; Planelles, J. Auger recombination suppression in nanocrystals with asymmetric electron-hole confinement. *Small* **2012**, *8*, 754−759.
(122) Bae, W. K.; Padilha, L. A.; Park, Y.-S.; McDaniel, H.; Robel, I.; Pietryga, J. M.; Klimov, V. I. Controlled alloying of the core-shell interface in CdSe/CdS quantum dots for suppression of Auger recombination. *ACS Nano* **2013**, *7*, 3411−3419.
(123) Park, Y.-S.; Lim, J.; Makarov, N. S.; Klimov, V. I. Effect of interfacial alloying versus "volume scaling" on Auger recombination in compositionally graded semiconductor quantum dots. *Nano Lett.* **2017**, *17*, 5607−5613.
(124) Lim, J.; Park, Y.-S.; Klimov, V. I. Optical gain in colloidal quantum dots achieved with direct-current electrical pumping. *Nat. Mater.* **2018**, *17*, 42−49.
(125) Lim, J.; Park, Y.-S.; Wu, K.; Yun, H. J.; Klimov, V. I. Droop-free colloidal quantum dot light-emitting diodes. *Nano Lett.* **2018**, *18*, 6645−6653.
(126) García de Arquer, F. P.; Talapin, D. V.; Klimov, V. I.; Arakawa, Y.; Bayer, M.; Sargent, E. H. Semiconductor quantum dots: Technological progress and future challenges. *Science* **2021**, *373*, eaaz8541.

https://doi.org/10.1021/acsnano.4c09833
ACS Nano 2024, 18, 35104−35118